Periodic perturbation of a 3D conservative flow with a heteroclinic connection to saddle-foci

A. Murillo[1] and A. Vieiro[1,2]

[1]Departament de Matemàtiques i Informàtica, Universitat de Barcelona (UB), Gran Via, 585, 08007 Barcelona, Spain
[2]Centre de Recerca Matemàtica (CRM), Campus Bellaterra, 08193 Bellaterra, Spain

January 31, 2025

Keywords: Hopf-zero bifurcation, splitting of separatrices, exponentially small phenomena, quasi-periodic phenomena

Abstract

The 2-jet normal form of the elliptic volume-preserving Hopf-zero bifurcation provides a one-parameter family of volume-preserving vector fields with a pair of saddle-foci points whose 2-dimensional invariant manifolds form a 2-sphere of spiralling heteroclinic orbits. We study the effect of an external periodic forcing on the splitting of these 2-dimensional invariant manifolds. The internal frequency (related to the foci and already presented in the unperturbed system) interacts with an external one (coming from the periodic forcing). If both frequencies are incommensurable, this interaction leads to quasi-periodicity in the splitting behaviour, which is exponentially small in (a suitable function of) the unfolding parameter of the Hopf-zero bifurcation. The corresponding behaviour is described by a Melnikov function. The changes of dominant harmonics correspond to primary quadratic tangencies between the invariant manifolds. Combining analytical and numerical results, we provide a detailed description of the asymptotic behaviour of the splitting under concrete arithmetic properties of the frequencies.

1 Introduction

In the last years there has been an increasing dynamical interest in three-dimensional (3D) flows [18, 24, 30]. This was highly motivated by the fact that, in general, that is without having extra symmetries allowing further dimensional reduction, the velocity vector field of a fluid defines a 3D flow. Unsteady fluid flows, in which the conditions (the velocity, the pressure and the cross-section) change over time, lead to time-dependent perturbations of the vector fields. Volume-preserving rotational symmetry breaking and periodic perturbations of 3D conservative flows (and/or 3D volume-preserving maps) have been suggested to model periodically time-dependent velocity fields in incompressible fluid flows and have been studied both theoretically and experimentally [31, 42, 43]. The role of the separatrix surface in the transport and mixing properties of the 3D flows has been considered in different related settings and applications, see [33, 36, 35, 45], for example.

In this work, we study the effect of a periodic forcing on the splitting of the 2-dimensional separatrices of the 2-jet of a one-parameter family of 3-dimensional vector fields of the unfolding of the volume-preserving elliptic Hopf-zero bifurcation. In the scenario we consider, the bifurcation gives rise to a pair of saddle-foci equilibria whose 2-dimensional invariant manifolds form an invariant 2-sphere of spiralling heteroclinic orbits. The 2-jet commutes with the group of rotations that fix the axis joining these points. Hence, the unperturbed system has a natural (internal) frequency which, without losing generality, can be assumed to be normalized to one. The periodic forcing adds a second (external) frequency to the system.

The effect of the periodic forcing creates a splitting between the 2D invariant manifolds of the saddle-foci equilibria. In the analytic category, such splitting behaves exponentially small in (a power of) the unfolding parameter ε from the Hopf-zero bifurcation. When the size of the internal and the external frequencies are comparable, their interaction leads to quasi-periodic effects in the exponent of the exponentially small in ε asymptotic behaviour of the splitting of these invariant manifolds. Note that the scenario here considered is of the lowest possible dimension to have such an interaction of internal and external frequencies.

The paper is organized as follows. In Section 2 we introduce the system and the details of the perturbation. Some preliminary numerical computations of the 2D invariant manifolds and their splitting are given in Section 3. Section 4 is devoted to the derivation and analysis of the Melnikov function. The forcing considered resembles that of [20] in a different context but the study of the Melnikov function properties in Section 4 is simpler for the system here considered. In particular, we consider the leading terms of the Melnikov function and, in Appendix A, we provide explicit bounds of the contribution of the remaining terms to the amplitude of the Melnikov function. Moreover, different scenarios are considered depending on the analytical properties of the perturbation and we give explicit expressions of the asymptotic behaviour of the amplitude of the splitting expected in each case. Some numerical explorations of the Melnikov function in Section 4.3 illustrate different possible behaviours depending on the arithmetic properties of the interacting frequencies. These results are analytically justified in Section 4.4. Moreover, in Section 5 we show that the changes in the homology of the nodal lines of the Melnikov function, due to changes of its leading harmonics, correspond to quadratic tangencies of saddle type between the 2-dimensional invariant manifolds of the saddle-foci equilibria. The sequence of parameters ε for which the family of systems considered show such tangencies accumulate to $\varepsilon = 0$ at a ratio depending on the arithmetic properties of the system, see Theorem 5.1 for a precise statement. Finally, Section 6 considers the asymptotic behaviour of some local quantities that measure the splitting of the 2D invariant manifolds of the saddle-foci points of the system.

2 The vector field model and its relation with the Hopf-zero bifurcation

We consider a three-dimensional conservative system of differential equations defined by a vector field X of the form $X(x, y, z, t) = X_0(x, y, z) + \delta X_1(x, y, z, t)$, where the perturbation δX_1 is a $2\pi/\omega$-periodic in time forcing of an autonomous integrable vector field X_0. We are interested in a very specific phase space configuration of the unperturbed system defined by X_0. In particular, we assume that the unperturbed system has a bubble structure. To better describe this structure let us first introduce the model that we are going to consider and discuss the phenomena that we want to study.

The concrete system is given by the vector field

$$X(x,y,z,t) = X_0(x,y,z) + \delta X_1(x,y,z,t), \tag{1}$$

where

$$X_0(x,y,z) = \left(y - xz,\ -x - yz,\ -\varepsilon^2 + z^2 + \frac{1}{2}(x^2+y^2) \right)^\top, \tag{2}$$

and

$$X_1(x,y,z,t) = \left(0,\ 0,\ \frac{y(x^2+y^2)}{2(c-y)} \frac{\tilde{g}(\psi)}{d-\cos(\psi)} \right)^\top, \qquad \psi(t) = \omega t + \psi_0,$$

with parameters $c, d, \varepsilon, \delta, \omega \in \mathbb{R}$ and an initial time phase $\psi_0 \in [0, 2\pi)$. To simplify notations, we omit the dependence of X on those parameters. The function $\tilde{g}(\psi)$ is considered to be a trigonometric polynomial. For concreteness, we mainly consider $\tilde{g}(\psi) \equiv 1$, but we also include some explorations considering $\tilde{g}(\psi) = \sin(\psi)$ to stress their differences. Perturbations with other trigonometric functions $\tilde{g}$ can be similarly handled. Moreover, we restrict to values of $c > 2\varepsilon$ and $d > 1$ to guarantee that there is $\nu > 4$ so that X is analytic in the cylindrical domain

$$\mathcal{D} = \{(x,y,z,\psi) \in \mathbb{R}^4,\ x^2 + y^2 < \nu\varepsilon^2\} \subset \mathbb{R}^3 \times \mathbb{R}/2\pi\mathbb{Z}, \tag{3}$$

where we study the associated system.

The study we perform depends on both the forcing parameter $\delta \geq 0$ and the bifurcation parameter $\varepsilon > 0$. At the limit $\varepsilon \to 0$, the vector field X_0 approaches a bifurcation that causes a change in the topology of the phase space we are interested in (see details in Section 2.1). Then, our analytical results for X are perturbative on δ, and provide a description of the exponentially small phenomena for any sufficiently small fixed value of δ when $\varepsilon \to 0$. The range of values of δ for which our approach provides an accurate description depends on the properties of the perturbation X_1.

The phenomena we are interested in strongly depend on the interaction between the unperturbed system X_0, which corresponds to $\delta = 0$, and the perturbation X_1, mainly through the arithmetic properties of $\omega \in \mathbb{R} \setminus \mathbb{Q}$. The concrete forms of X_0 and X_1 are chosen to simplify the computations and allow visualizations. However, the same phenomena are expected for more general perturbations if they interact with an unperturbed system with a similar phase space structure as the system defined by X_0. Also, as suggested in Section 6, similar phenomena are expected for families of near-integrable volume-preserving maps.

2.1 The phase space structure of the unperturbed system

For $\varepsilon > 0$, the unperturbed system X_0 has two equilibria $p_\pm = (0, 0, \pm\varepsilon)$ of saddle-foci type, with stable and unstable invariant manifolds satisfying $\dim W^u(p_+) = \dim W^s(p_-) = 1$ and $\dim W^s(p_+) = \dim W^u(p_-) = 2$, since $\mathrm{Spec}(DX(p_\pm)) = \{\pm 2\varepsilon, \mp\varepsilon + \mathrm{i}, \mp\varepsilon - \mathrm{i}\}$.

The 2D invariant manifolds of $p_\pm$ coincide and form an invariant ellipsoid $\{z^2 + (x^2+y^2)/4 = \varepsilon^2\}$, which is foliated by the one-parameter family of heteroclinic orbits

$$\gamma(t, \theta_0, \varepsilon) = \left(2\varepsilon\,\mathrm{sech}(\varepsilon t)\cos(-t+\theta_0),\ 2\varepsilon\,\mathrm{sech}(\varepsilon t)\sin(-t+\theta_0),\ \varepsilon\tanh(\varepsilon t)\right)^\top, \tag{4}$$

where $\theta_0 \in [0, 2\pi)$ is an arbitrary phase. In particular, $\gamma(t, \theta_0, \varepsilon)$ has singularities at $t = (\pi i + 2\pi i k)/2\varepsilon, k \in \mathbb{Z}$.

Moreover, the unperturbed system X_0 admits the integrating factor $\mu(x,y) = 2(x^2+y^2)$ on $\mathbb{R}^3 \setminus \{x = y = 0\}$ and then μX_0 has

$$H_\varepsilon(x,y,z) = (x^2+y^2)\left(-\varepsilon^2 + z^2 + \frac{x^2+y^2}{4}\right), \tag{5}$$

as a first integral. By continuity, it can be extended to the invariant axis $x = y = 0$. We shall use H_ε to compute the Melnikov function and measure the splitting of the 2D invariant manifolds, in Section 4.

Using polar coordinates in the (x,y)-plane the unperturbed system X_0 becomes

$$\dot{r} = -rz, \quad \dot{\theta} = -1, \quad \dot{z} = -\varepsilon^2 + z^2 + r^2/2.$$

Due to the uncoupled structure, we can study the evolution of the (z,r) coordinates independently. The unperturbed system possesses a rotational symmetry, with an (internal) rotation frequency which is equal to -1. It is invariant by elements of the group of rotations $e^{\theta L_z}$ that keep the z-axis invariant. The first integral

$$H_\varepsilon(z,r) = r^2\left(-\varepsilon^2 + z^2 + \frac{r^2}{4}\right), \tag{6}$$

induces a foliation by constant level sets, which is transversal to the regular foliation that defines the action of the group of rotations generated by L_z.

In Fig.1 we can observe the main features of the reduced (z,r)-system. It has two saddle-type fixed points, $(\pm\varepsilon, 0)$, with three different one-dimensional heteroclinic connections. One of these connections lies on the z-axis, which is invariant by the system. The other two heteroclinic bound two regions that are foliated by periodic orbits and contain two elliptic fixed points $(0, \pm\sqrt{2}\varepsilon)$. Taking into account the action of the rotation group $\langle L_z \rangle$, we can conclude that the periodic orbits observed in the figure are two-dimensional invariant tori of the 3D integrable system X_0. On the other hand, the heteroclinic connections not contained in the invariant z-axis correspond to 2D heteroclinic connections to the saddle-foci equilibria of X_0. The structure that bound the 2D heteroclinic connections, along with the foliation by 2D tori contained within, is usually referred to as a bubble of stability.

For 3D flows, such a bubble structure is, generically, created at a Hopf-zero bifurcation. There are six different topological types of Hopf-zero singularities [44]. For a particular topological type, the Hopf-zero singularity bifurcates into a pair of saddle-foci and, for suitable parameters of the unfolding, their unstable and stable two-dimensional manifolds form an invariant ellipsoid, hence a bubble of stability is created. The study of generic codimension two unfoldings of Hopf-Zero bifurcations started with the works by Guckenheimer and Gavrilov, [22, 21]. A fairly exhaustive list of references containing additional developments of the Hopf-zero bifurcation is provided in [2] where the authors considered the same topological type of Hopf-zero singularity that we are interested in and prove that a generic unfolding has Shilnikov homoclinic orbits.

The unperturbed vector field X_0 is obtained as the second-order truncation of the normal form of the volume-preserving unfolding of the Hopf-Zero singularity at $\varepsilon = 0$. More concretely, for $\varepsilon > 0$ the unperturbed phase space shows a bubble structure of size $\mathcal{O}(\varepsilon)$ that collapses to the origin, which is the unique parabolic equilibrium point of the system X_0 for $\varepsilon = 0$ and disappears for $\varepsilon < 0$.

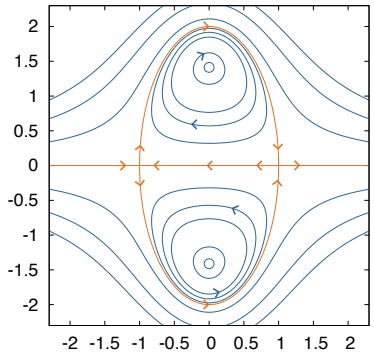

Figure 1: Phase space of the reduced 2D (z, r)-system for $\varepsilon = 1$, where three heteroclinic orbits between saddle equilibria bound two elliptic regions that lead to the 3D stability bubble.

2.2 The perturbed system

We proceed by adding the periodic forcing δX_1 to X_0 in (2). We express the forcing as

$$X_1(x, y, z, t) = \left(0,\ 0,\ \frac{y(x^2 + y^2)}{2} f(y) g(\psi)\right)^\top,$$

where $f(y) = 1/(c - y)$, $g(\psi) = \tilde{g}(\psi)/(d - \cos(\psi))$, and $\psi = \omega t + \psi_0$. X_1 is a third-order conservative perturbation that vanishes at $p_\pm = (0, 0, \pm\varepsilon)$ and, independently of the values of the parameters, preserves the saddle-foci type of the equilibria. On the other hand, the invariant manifolds remain but do not coincide. Additionally, this perturbation breaks the symmetry of the normal form, since $y(x^2 + y^2)$ is not a resonant term.

The 3D vector field $X = X_0 + \delta X_1$ is non-autonomous, and, on the extended phase space $\mathcal{D} \subset \mathbb{R}^3 \times \mathbb{S}^1$, defined in (3), the system becomes autonomous. The corresponding vector field $\hat{X}$ is given by

$$\hat{X}(x, y, z, \psi) = \hat{X}_0(x, y, z) + \delta \hat{X}_1(x, y, z, \psi), \tag{7}$$

where $\hat{X}_0(x, y, z) = (X_0(x, y, z), \omega)$ and $\hat{X}_1(x, y, z, \psi) = (X_1(x, y, z, t), 0)^\top$. If $\tilde{g}(\psi)$ is an even function, $\hat{X}$ is reversible. Recall that a vector field $Y : M \to TM$ defined on a differentiable manifold M is reversible with respect to an involution $R : M \to M$ if $DR(Y(x)) = -Y(R(x))$, for all $x \in M$. In particular, the vector field $\hat{X}$ is R-reversible with

$$R(x, y, z, \psi) = (-x, y, -z, -\psi).$$

It follows that $R(\phi^t(x, y, z, \psi)) = \phi^{-t}(R(x, y, z, \psi))$ where ϕ^t denotes the flow of $\hat{X}$.

We aim to study the asymptotic behaviour, as $\varepsilon \to 0$, of the splitting of the 2D heteroclinic invariant manifold that bounds the bubble of X_0 when considering $\delta > 0$ small. Even though in theoretical considerations we are not restricted to these specific values, the computations reported in this manuscript correspond to the extended system $\hat{X}$ with

$$c = 0.5, \quad d = 5 \quad \text{and} \quad \delta = 10^{-2},$$

unless otherwise explicitly specified. The frequency ω is usually assumed to be $\sqrt{2}$ and $\tilde{g}(\psi) = 1$.

Expressing the extended system in the (r, z, θ, ψ) coordinates and rescaling $r = \hat{r}\varepsilon$, $z = \hat{z}\varepsilon$ and $t\varepsilon = \hat{t}$, one obtains

$$\hat{r}' = -\hat{r}\hat{z}, \quad \hat{z}' = -1 + \hat{z}^2 + \frac{\hat{r}^2}{2}\left(1 + \delta\varepsilon\,\hat{r}\sin(\theta) f(\varepsilon\hat{r}\sin(\theta)) g(\psi)\right), \quad \theta' = -\frac{1}{\varepsilon}, \quad \psi' = \frac{\omega}{\varepsilon}, \tag{8}$$

where $' = d/d\hat{t}$. We see that, for $\omega \in \mathbb{R} \setminus \mathbb{Q}$, the system is a fast quasi-periodic perturbation, in $(\theta, \psi) \in \mathbb{T}^2 \simeq (\mathbb{R}/(2\pi\mathbb{Z}))^2$, of a planar one. The Fourier expansion of the perturbation has harmonics of all orders in both θ and ψ.

The decay of the Fourier coefficients function is related to the width of its analytic strip. The function $f(r\sin(\theta))$ is analytic in the complex strip $\{\theta \in \mathbb{C}, \mathrm{Re}(\theta) \in \mathbb{T}, |\mathrm{Im}(\theta)| < \rho_\theta\}$ given by $\rho_\theta = \mathrm{arcsinh}(c/\sqrt{\nu\varepsilon})$, where $\nu > 4$ determines the domain $\mathcal{D}$. On the other hand, $g(\psi)$ is analytic in the complex strip $\{\psi \in \mathbb{C}, \mathrm{Re}(\psi) \in \mathbb{T}, |\mathrm{Im}(\psi)| < \rho_\psi\}$ with $\rho_\psi = \mathrm{arccosh}(d)$.

Given $d > 1$, if one considers $c > 2\varepsilon$ such that $\varepsilon/c \to 0$ as $\varepsilon \to 0$, then the function $f(r\sin(\theta))$ converges to an entire function as $\varepsilon \to 0$. A perturbation of the form $f(y)g(\psi)$ with f an entire function was considered in [16]. However, if one considers c depending on ε as $c = c(\varepsilon) = \tilde{c}\varepsilon$, then the strip of analyticity of f tends to some constant width as $\varepsilon \to 0$. Finally, we also note that, for $\tilde{g}(\psi) \equiv 1$, $g(\psi)$ is an even function and, in this case, the splitting function differs from the general case. A perturbation $f(y)g(\psi)$ with f analytic on a finite strip domain and the same even function g was considered in [20] in a different context. We refer to Section 4 for comments on the consequences of the different decays of Fourier coefficients in the splitting. The influence of the parity of $g(\psi)$ will be also discussed.

3 Parameterization of the invariant manifolds, heteroclinic orbits and splitting

As already stated, our main interest in this work concerns the splitting of the 2D invariant manifolds of $p_\pm$. For the unperturbed system (2), the invariant manifolds $W^u(p_-)$ and $W^s(p_+)$ coincide (and bound a bubble of stability). However, for $\delta > 0$, the perturbation is expected to cause the splitting of these invariant manifolds. To understand the splitting of these manifolds we start by, in this section, investigating it numerically. To this end, we fix $\delta > 0$ small and, for a sequence of values of ε approaching zero, we numerically compute the invariant manifolds and measure their splitting on $\Sigma = \{z = 0\}$. Note that Σ is transversal to $\hat{X}$ near the invariant manifolds for δ small enough.

To measure the splitting on Σ we first obtain a local representation of the invariant manifolds and then we propagate them up to Σ by numerical integration of the vector field. As we explain below, we use the parameterization method to get the local representation of the invariant manifolds [4, 5, 6, 23] and a Taylor integrator to carry out the propagation step, see for example [26]. As the splitting behaviour turns out to be exponentially small in ε, the computations need to be carried out with extended precision. Implementations were done in pari/gp [3], hence using the gmp library for extended precision arithmetics, to this end.

To compute a local approximation of the 2D invariant manifolds of the fixed points $p_\pm$ we look for parameterizations $K^{u,s}(s, \overline{s}, \psi)$ of the unstable and stable manifolds as embeddings tangent to the two-dimensional eigenspace generated by the eigenvectors of $D\hat{X}(p_\pm)$ at $p_\pm$, see [20, 32]. This leads to the so-called invariance equation,

$$\hat{X}(K^{u,s}(s, \overline{s}, \psi), \psi) = D_{s,\overline{s}}K^{u,s}(s, \overline{s}, \psi)\Lambda(s, \overline{s}) + D_\psi K^{u,s}(s, \overline{s}, \psi)\omega, \tag{9}$$

where $\Lambda : \mathbb{R}^2 \longrightarrow \mathbb{C}^2$ is the vector field associated to the eigenvectors of $D\hat{X}(p_\pm)$, defined as $\Lambda(s_1, s_2) = (\mu s, \overline{\mu s})$, where $\mu = \mp\varepsilon + \mathrm{i}$ is an eigenvalue of $D\hat{X}(p_\pm)$ and $s = s_1 + \mathrm{i}\, s_2$. The parameterization $K^{u,s}(s, \overline{s}, \psi)$ is a sum of homogeneous polynomials on s and $\overline{s}$, where the coefficients are smooth functions depending on the time variable ψ. But since $K^{u,s}(s, \bar{s}, \psi) =$

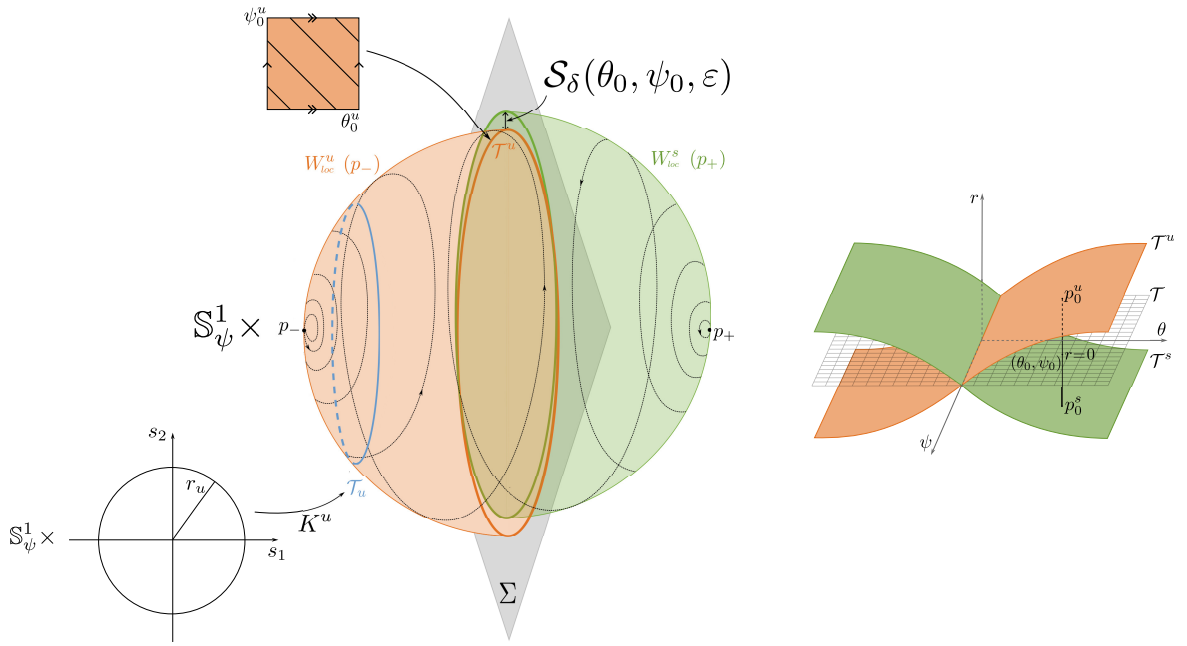

Figure 2: A representation of the coordinates introduced is sketched in the left plot. In the (z,x,y)-projection shown, the torus $\mathcal{T}^u$ is the circle $W^u(p_-)\cap\Sigma$. The splitting function $\mathcal{S}_\delta$ measures a radial distance, between $\mathcal{T}^u$ and $\mathcal{T}^s$ by computing the difference of the Hamiltonian energy H_ε at pairs of points with same coordinates $(\theta,\psi)\in\mathcal{T}$. This is schematically represented in the (θ,ψ,r)-projection shown in the right plot.

$K_2^{u,s}(s,\bar{s})+\mathcal{O}\left((s+\bar{s})^3e^{i\psi}\right)$ for all $\psi\in[0,2\pi)$, we truncate the parameterization to second order to avoid dealing with Fourier expansions in ψ when solving (9). As a counterpart, $K_2^{u,s}(s,\bar{s})$ gives an accurate representation of $W^{u,s}_{\rm loc}(p_\pm)$ just for relatively small $|s|$. The local tolerance imposed in (9) and the corresponding maximum value of $|s|$ are adjusted for each value of the parameter ε to reach Σ with enough accuracy after the propagation step (also the order and local error of the Taylor time-stepper is adapted to this end).

Denote by r_u the maximum value of $|s|$ up to which $K_2^u(s,\bar{s})$ gives an accurate representation of $W^u_{\rm loc}(p_-)$. Introducing $s=r_ue^{i\theta}$, $\theta\in[0,2\pi)$, we identify $W^u_{\rm loc}(p_-)\cap\{|s|=r_u\}$ with the 2D torus $\mathcal{T}_u\subset\mathbb{R}^3\times\mathbb{S}^1$ given by

$$\mathcal{T}_u=\{(x,y,z,\psi)\in\mathbb{R}^3\times\mathbb{S}^1,(x,y,z)=K_2^u(s,\bar{s}),s=r_ue^{i\theta},\theta\in[0,2\pi),\psi\in[0,2\pi)\}.$$

Let $\mathcal{T}^u$ be the torus obtained by the propagation of the points of $\mathcal{T}_u$ up to Σ under the flow ϕ^t of the system (7). See the sketch in Fig. 2 left. It is convenient to introduce coordinates (r,θ,ψ) in Σ through the relations $\theta=\text{atan2}(y,x)$, $r=\sqrt{x^2+y^2}$ and $\psi=\omega t\ (\text{mod}2\pi)$. Then, given $(\theta_u,\psi_u)\in[0,2\pi)\times[0,2\pi)$ we get a point $p_u\in\mathcal{T}_u$ that is considered as initial condition and propagated under the flow ϕ^t of (7) until reaching Σ. In this way we get a point $p_0^u=(\theta_0^u,r_0^u,\psi_0^u)\in\mathcal{T}^u=W^u(p_-)\cap\Sigma$, where (θ_0^u,r_0^u) are polar coordinates of (x_0^u,y_0^u) in $z=0$. By analogy, we denote $\mathcal{T}_s$, $\mathcal{T}^s$ and p_0^s the corresponding definitions related with $W^s(p_+)$.

Note that for $\tilde{g}(\psi)=1$, the extended system is R-reversible and $R(W^u(p_-))=W^s(p_+)$, so that one can compute $W^u(p_-)$ and apply the reversibility to obtain $W^s(p_+)$, significantly reducing the total computational cost. Then, the point $R(p_0^u)$ is on the 2D torus $\mathcal{T}^s=R(\mathcal{T}^u)$. However, in order to compute the splitting between the invariant manifolds $W^u(p_-)$ and $W^s(p_+)$ on the Poincaré section $\Sigma=\{z=0\}$ we would like to express both invariant manifolds as a graph over

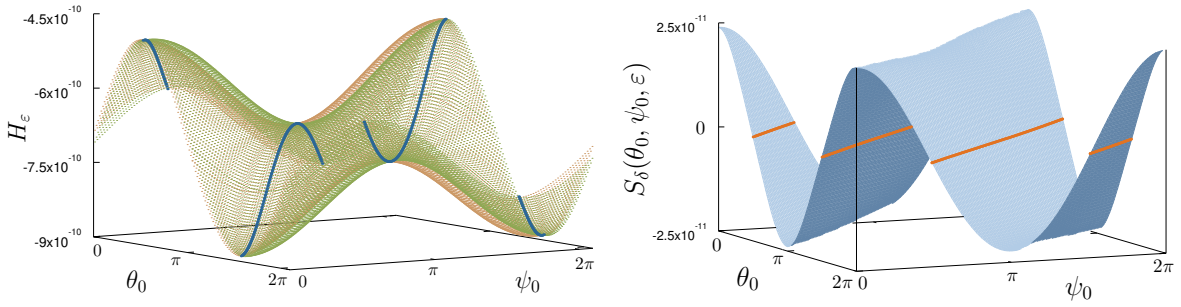

Figure 3: For $\varepsilon = 0.05$, we display in the left plot the stable and unstable invariant manifolds (green and orange respectively) and the continuum of heteroclinic orbits (in blue). In the right plot, we display the splitting function and the nodal lines, corresponding to the continuum of heteroclinic orbits.

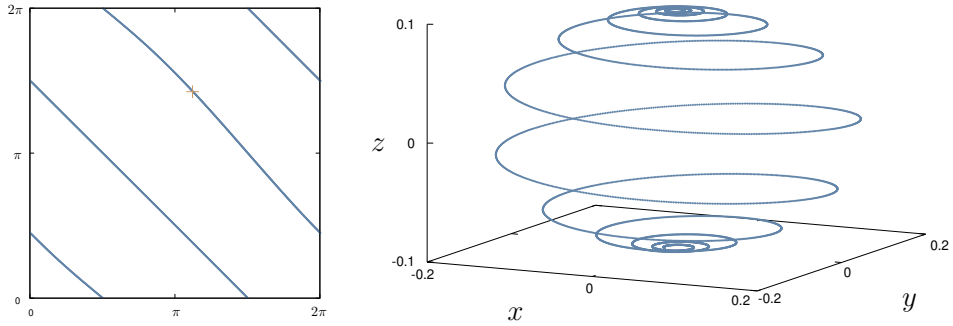

Figure 4: We display the nodal lines of S_δ for $\varepsilon = 0.1$. The right plot shows the heteroclinic orbit $(\theta_0, \psi_0) = (3.52, 4.47)$, shown in orange in the left plot.

angle coordinates (θ_0, ψ_0), a fundamental torus $\mathcal{T}$, so that we can compute the radial distance between points sharing the same angle coordinates. See Fig. 2 right. To this end, for the fixed small value of $\delta > 0$ and a given $\varepsilon > 0$, we select an equispaced mesh of angles $(\theta_0, \psi_0) \in \mathcal{T}$ and refine (θ_u, ψ_u) (resp. (θ_s, ψ_s)), using a Newton method, to guarantee that we reach the point $p_0^u \in \mathcal{T}^u$ (resp. $p_0^s \in \mathcal{T}^s$) with the desired angle coordinates $(\theta_0, \psi_0) \in \mathcal{T}$. Then we define the splitting function to be

$$\mathcal{S}_\delta(\theta_0, \psi_0, \varepsilon) = H_\varepsilon(p_0^u) - H_\varepsilon(p_0^s), \tag{10}$$

where H_ε is the first integral of the unperturbed system X_0, defined in (5).

In the left plot of Fig.3 we display $W^u(p_-)$, in orange, and $W^s(p_+)$, in green, for $\varepsilon = 0.05, \delta = 0.01$ and $\omega = \sqrt{2}$. At the scale of the figure, both invariant manifolds are difficult to distinguish, so in the right plot we display the results of the direct computation (that is, based on the numerical computation of the local invariant manifolds and their propagation until reaching Σ) of the splitting function $\mathcal{S}_\delta(\theta_0, \psi_0, \varepsilon)$, as given by (10), to illustrate their difference.

Given $\varepsilon > 0$, each point on the set of nodal lines $\mathcal{S}_\delta(\theta_0, \psi_0, \varepsilon) = 0$ corresponds to a heteroclinic orbit between p_- and p_+. The nodal lines in the plane $\{z = 0\}$ can be numerically obtained using a Newton method to compute (θ_u, ψ_u) and (θ_s, ψ_s) such that $p_0^u = p_0^s$. The blue curves shown in Figure 3 left correspond to points where $\mathcal{S}_\delta(\theta_0, \psi_0, \varepsilon) = 0$, shown in orange in the right plot. The nodal lines on the fundamental torus at $\{z = 0\}$ are shown in Fig.4 left. The marked point on the nodal line is a representant on $\{z = 0\}$ of the heteroclinic orbit shown in the right plot.

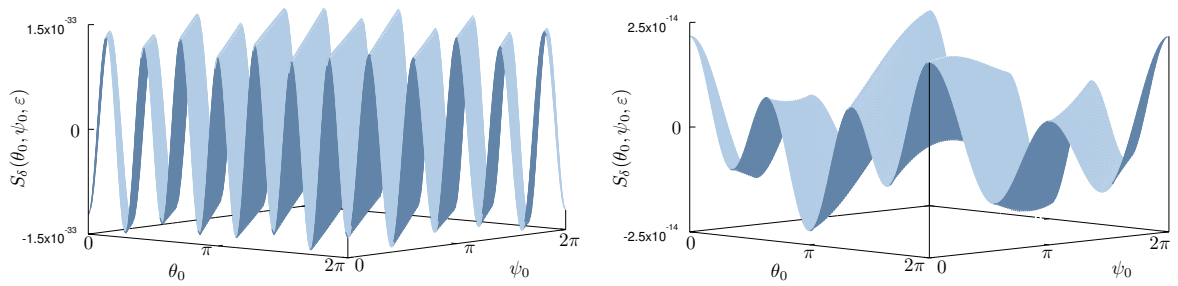

Figure 5: Splitting function with respect to (θ_0, ψ_0) for a fixed $\delta = 0.01$ and $\omega = \sqrt{2}$ and $\varepsilon = 0.005$ and 0.03125.

In Fig.5 we display the splitting function for different values of ε. We see that for smaller values of ε the splitting function has more oscillations. In the next section, we describe the splitting function through a first-order Poincaré-Melnikov approximation. The asymptotic behaviour of the nodal lines will be discussed in Section 5.

4 The Melnikov function: changes in the dominant harmonic

In this section, we derive the first-order Poincaré-Melnikov approximation with respect to the periodic forcing parameter $\delta > 0$ of the splitting function $S_\delta(\theta_0, \psi_0, \varepsilon)$ defined in (10). Furthermore, we also show that the dominant terms of this approximation are enough to understand the asymptotic behaviour of the splitting of the 2D invariant manifolds. Additionally, we illustrate the role of the analytic properties of the unperturbed separatrix and the perturbation in the expected size of the splitting when $\varepsilon \to 0$. The changes in the dominant harmonic and the topology of these changes will be analysed in the next section.

Even though the Poincaré-Melnikov approximation has not been theoretically justified to hold in this context, similar computations in analogous examples support the use of such approximation in this setting. We refer to [39, 11, 16, 40] for analytical and numerical studies based on the Poincaré-Melnikov approximation in the context of invariant manifolds of invariant tori in 2-dof Hamiltonian systems. In particular, comparison with direct computations shows an excellent agreement as we will also illustrate for the model under consideration here, see also [19]. We refer to [12, 13, 14] for the more involved setting where the quasi-periodic forcing has three frequencies.

4.1 Derivation of the Poincaré-Melnikov approximation

The splitting function $S_\delta(\theta_0, \psi_0, \varepsilon)$ defined in (10) measures the radial distance between two points $p_0^u \in \Sigma \cap W^u(p_-)$ and $p_0^s \in \Sigma \cap W^s(p_+)$ that have the same (θ_0, ψ_0) coordinates. Those points depend on the bifurcation parameter ε and the forcing parameter δ, the notation here emphasizes the dependence on the last one.

Given (θ_0, ψ_0), let $\phi(t; p_0^{u,s}(\delta), \delta) \in \mathbb{R}^3$ be the solution at time t of the non-autonomous system

$X = X_0 + \delta X_1$ that starts at $p_0^{u,s}$. Expanding the solution around $\delta = 0$ one obtains

$$\begin{aligned}\mathcal{S}_\delta(\theta_0, \psi_0, \varepsilon) &= H_\varepsilon(p^u(\delta)) - H_\varepsilon(p^s(\delta)) = \\ &= \delta \int_{-\infty}^{\infty} DH_\varepsilon(\gamma(t, \theta_0, \varepsilon)) X_1(\gamma(t, \theta_0, \varepsilon), t) dt + O(\delta^2) = \delta M(\theta_0, \psi_0, \varepsilon) + O(\delta^2),\end{aligned}$$

where $\gamma(t, \theta_0, \varepsilon) = \phi(t; p^{u,s}(0), 0)$ is the corresponding heteroclinic orbit[1] of the unperturbed system X_0 defined in (4). Here $M(\theta_0, \psi_0, \varepsilon)$ is the so-called Poincaré-Melnikov approximation and it is given by the Melnikov integral

$$M(\theta_0, \psi_0, \varepsilon) = \int_{-\infty}^{\infty} z_\gamma(t)(x_\gamma^2(t) + y_\gamma^2(t))^2 \, y_\gamma(t) f(y_\gamma(t)) g(\psi) dt,$$

where $(x_\gamma, y_\gamma, z_\gamma)$ are the components of the heteroclinic orbit $\gamma(t, \theta_0, \varepsilon)$ and $\psi = \omega t + \psi_0$.

To compute this integral, consider $z_\gamma(t)(x_\gamma(t)^2 + y_\gamma(t)^2)^2 = 16\,\varepsilon^5 \, \frac{\sinh(\varepsilon t)}{\cosh(\varepsilon t)^5}$ and expand the functions $y_\gamma(t) f(y_\gamma(t))$ and $g(\psi)$. Firstly,

$$y_\gamma(t) f(y_\gamma(t)) = \frac{y_\gamma(t)}{c - y_\gamma(t)} = \sum_{n=1}^{\infty} \frac{2^n \varepsilon^n}{c^n} \frac{\sin(\theta)^n}{\cosh^n(\varepsilon t)} = \sum_{n=1}^{\infty} \frac{2\varepsilon^n}{c^n \cosh^n(\varepsilon t)} \sum_{k=0}^{\lfloor \frac{n}{2} \rfloor} a_{n,k} f_{n,k}(\theta),$$

where $\theta = -t + \theta_0$ and $a_{n,k} = (-1)^{\lfloor \frac{n}{2} \rfloor - k} \binom{n}{k}$, for $k < n/2$, while $a_{n,n/2} = \frac{1}{2}\binom{n}{n/2}$. The functions $f_{n,k}(\theta)$ are defined as $\sin((n-2k)\theta)$ for odd n and $\cos((n-2k)\theta)$ otherwise.

On the other hand, recall that $g(\psi) = \tilde{g}(\psi)/(d - \cos(\psi))$. For concreteness we give the details for $\tilde{g}(\psi) \equiv 1$, but one proceeds similarly for $\tilde{g}(\psi) = \sin(\psi)$, see Remark (4.1). The Fourier coefficients of the function $g(\psi) = \sum_{m=0}^{\infty} d_m \cos(m\psi)$ are given by

$$d_0 = \frac{1}{\sqrt{d^2 - 1}}, \qquad d_m = \frac{2 d_0}{(d + \sqrt{d^2 - 1})^m}, \qquad \text{for } m \geq 1.$$

With these expansions, the Melnikov integral takes the form

$$M(\theta_0, \psi_0, \varepsilon) = \sum_{m=0}^{\infty} \sum_{n=1}^{\infty} \sum_{k=0}^{\lfloor \frac{n}{2} \rfloor} \frac{d_m 2^5 \varepsilon^{n+5} a_{n,k}}{c^n} \left[\int_{-\infty}^{\infty} \frac{\sinh(\varepsilon t) f_{n,k}(\theta) \cos(m\psi)}{\cosh^{n+5}(\varepsilon t)} dt \right].$$

Using basic identities we express the trigonometric functions that appear in the integral in terms of sin and cos functions involving σt, where $\sigma = (m\omega - (n-2k))$, and $\Phi = (n-2k)\theta_0 + m\psi_0$. In particular, all terms containing $\cos(\sigma t)$ will lead to zero integrals since, together with the hyperbolic term, they are odd functions. Hence, the Melnikov function can be expressed as

$$M(\theta_0, \psi_0, \varepsilon) = \sum_{m=-\infty}^{\infty} \sum_{n=1}^{\infty} \sum_{k=0}^{\lfloor \frac{n}{2} \rfloor} \frac{2^5 \varrho_d^{|m|} \varepsilon^{n+5} a_{n,k} \; g(\Phi)}{\sqrt{d^2 - 1} c^n} \int_{-\infty}^{\infty} \frac{\sinh(\varepsilon t) \sin(\sigma t)}{\cosh^{n+5}(\varepsilon t)} dt,$$

where $\varrho_d = (d + \sqrt{d^2 - 1})^{-1}$ and $g(\Phi)$ is defined as $\cos(\Phi)$ for odd n and $-\sin(\Phi)$ for even n.

Let $I(\sigma, p) = \int_{-\infty}^{\infty} \frac{\sinh(\varepsilon t) \sin(\sigma t)}{\cosh^p(\varepsilon t)} dt$. Note that for $\sigma = 0$, we have $I(0, p) = 0$. Otherwise, for $p \geq 1$, one can integrate by parts twice to obtain the following recurrence relation,

$$I(\sigma, p+2) = \frac{\sigma^2 + \varepsilon^2 (p-1)^2}{\varepsilon^2 p (p+1)} \, I(\sigma, p),$$

[1]Recall that for $\delta = 0$ the unperturbed system has a continuous foliation of heteroclinic orbits that can be parameterized by θ_0.

and use the residue theorem to express the integral $I(\sigma, p)$ as follows,

$$\int_{-\infty}^{\infty} \frac{\sinh(\varepsilon t)\sin(\sigma t)}{\cosh^p(\varepsilon t)} dt = \frac{\pi P_{p-1}(\sigma,\varepsilon)}{\varepsilon^p (p-1)! h(\sigma)},$$

where $h(\sigma) = \sinh\left(\frac{\sigma\pi}{2\varepsilon}\right)$ if p is odd and $h(\sigma) = \cosh\left(\frac{\sigma\pi}{2\varepsilon}\right)$ if p is even, and $P_m(\sigma,\varepsilon)$ satisfies the recurrence relation $P_m(\sigma,\varepsilon) = (\sigma^2 + \varepsilon^2(m-2)^2)P_{m-2}(\sigma,\varepsilon)$, with initial values $P_0 = 1$, $P_1 = \sigma$.

Then, as $p = n + 5$, the Melnikov function is written as,

$$M(\theta_0,\psi_0,\varepsilon) = \frac{2^5\pi}{\sqrt{d^2-1}} \sum_{m=-\infty}^{\infty} \sum_{n=1}^{\infty} \sum_{k=0}^{\lfloor \frac{n}{2} \rfloor} \frac{\varrho_d^{|m|} a_{n,k} P_{n+4}(\sigma,\varepsilon)}{c^n (n+4)!} \hat{F}(\Phi,\sigma),$$

where $\hat{F}(\Phi,\sigma) = \cos(\Phi)/\cosh(\frac{\sigma\pi}{2\varepsilon})$ if n is odd and $\hat{F}(\Phi,\sigma) = -\sin(\Phi)/\sinh(\frac{\sigma\pi}{2\varepsilon})$ if n is even.

Let $m_2 = m$ and $m_1 = n - 2k$, so that $\sigma = m_2\omega - m_1$ and

$$M(\theta_0,\psi_0,\varepsilon) = \sum_{m_2\in\mathbb{Z}} \sum_{m_1\geq 0} \hat{C}_{m_1,m_2}\, T(m_1\theta_0 + m_2\psi_0), \tag{11}$$

where $T(\alpha) = \cos(\alpha)$ if m_1 is odd and $T(\alpha) = \sin(\alpha)$ otherwise, and

$$\hat{C}_{m_1,m_2} = (-1)^{\lfloor \frac{m_1+3}{2} \rfloor} \frac{2^5\pi \varrho_d^{|m_2|}}{\sqrt{d^2-1} c^{m_1}} \sum_{i\geq 0} \frac{(m_1+2i)!}{c^{2i}(m_1+2i+4)!(m_1+i)!i!} \frac{1}{h(\sigma)} P_{m_1+2i+4}(\sigma,\varepsilon). \tag{12}$$

with $h(\sigma) = \cosh\left(\frac{\sigma\pi}{2\varepsilon}\right)$ if m_1 is odd and $h(\sigma) = \sinh\left(\frac{\sigma\pi}{2\varepsilon}\right)$ otherwise.

Remark 4.1. For $g(\psi) = \sin(\psi)$, similar computations lead to the following Melnikov function:

$$M(\theta_0,\psi_0,\varepsilon) = \sum_{m_2\in\mathbb{Z}} \sum_{m_1\geq 0} \frac{(-1)^{m_1+1}|\varrho_d^{|m_2+1|} - \varrho_d^{|m_2-1|}|}{2\varrho_d^{|m_2|}} \hat{C}_{m_1,m_2}\, G(m_1\theta_0 + m_2\psi_0),$$

where $G(\alpha) = \sin(\alpha)$ if m_1 is odd and $G(\alpha) = \cos(\alpha)$ otherwise.

We show in Fig.6 that the Poincaré-Melnikov approximation shows a good agreement with the direct computations of the splitting function, following the methodology described in Section 3. In particular we see that the difference between the splitting function and the Melnikov approximation is of order δ^2.

4.2 Amplitude of the harmonics associated with approximants of ω

Explicit bounds of the relative contribution to the total amplitude of the Melnikov function of the terms C_{m_1,m_2} such that $s = |m_2\omega - m_1| \leq \varepsilon$ or $s \geq \varepsilon^\alpha$ with $\alpha \leq 1/2 - \eta$, $\eta > 0$, are given in Appendix A (see Lemma A.3 and A.5). In particular, these terms can be ignored to study the leading terms of the Melnikov function that give the asymptotic behaviour of its amplitude when $\varepsilon \to 0$. Concretely,

$$\begin{aligned} |M(\theta_0,\psi_0,\varepsilon)| &\leq |M_{\varepsilon<s<\varepsilon^\alpha}(\theta_0,\psi_0,\varepsilon)| + |M_{s\leq\varepsilon}(\theta_0,\psi_0,\varepsilon)| + |M_{s\geq\varepsilon^\alpha}(\theta_0,\psi_0,\varepsilon)| \\ &\leq |M_{\varepsilon<s<\varepsilon^\alpha}(\theta_0,\psi_0,\varepsilon)| + O(\exp(-1/\varepsilon)) + O(\exp(-1/\varepsilon^{1/2+\eta})). \end{aligned}$$

The leading terms of the Melnikov function are given by pairs (m_1, m_2) related to linear combinations of the frequencies $(1,\omega)$ such that $s = |m_2\omega - m_1|$ lies in the strip $\varepsilon < s < \varepsilon^\alpha$. Below we restrict to (m_1, m_2) in this s-strip.

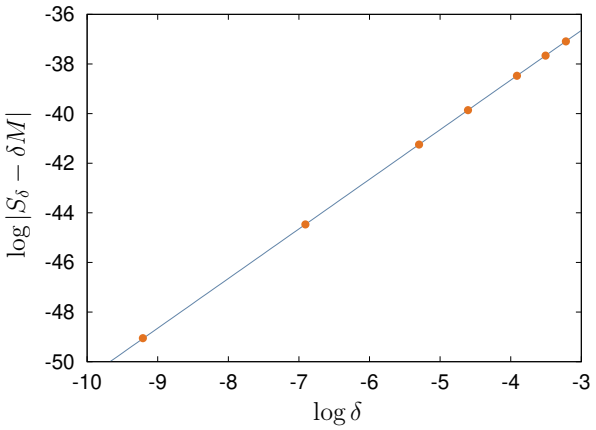

Figure 6: The points show the difference between the splitting function (numerically calculated from the computation of the invariant manifolds) and the Poincaré-Melnikov approximation (calculated by truncation of expansion (11)) for different values of δ and $\varepsilon = 0.03125$ fixed. We add for reference a fit of a line with slope equals 2, in agreement with the approximation $S_\delta = \delta M + O(\delta^2)$.

For s/ε sufficiently large, we can approximate $1/h(s)$ by $2\exp\left(-\frac{s\pi}{2\varepsilon}\right)$ and so, the amplitude of the Fourier modes of $M(\theta_0, \psi_0, \varepsilon)$ is given by

$$C_{m_1,m_2} = |\hat{C}_{m_1,m_2}| \approx \frac{2^6\pi\varrho_d^{|m_2|}}{\sqrt{d^2-1}c^{m_1}} \exp\left(\frac{-s\pi}{2\varepsilon}\right) S_A \tag{13}$$

where

$$S_A = \sum_{i\geq 0} A_i, \qquad \text{and} \qquad A_i = \frac{(m_1+2i)!}{c^{2i}(m_1+i)!(m_1+2i+4)!i!} P_{m_1+2i+4}(s).$$

We recall that $s = |m_2\omega - m_1|$, $\varrho_d = (d+\sqrt{d^2-1})^{-1}$ and $P_m(s,\varepsilon) = (s^2+\varepsilon^2(m-2)^2)P_{m-2}(s,\varepsilon)$, with $P_0 = 1, P_1 = s$.

The s-strip considered mainly contains some of the (m_1, m_2)-harmonics related to best approximants of ω. Other terms related to approximants m_1/m_2 of ω which are not best approximants also fall into the s-strip because of the bounds used for the s-width of the region containing the dominant terms of the Melnikov function. In ranges where one harmonic dominates, the optimal bound is $\mathcal{O}(\sqrt{\varepsilon}\log(\varepsilon))$ when the function f of the perturbation X_1 is entire, see details in Section 4.4. In Fig. 7 we consider two consecutive best approximants, $(41, 29)$ and $(99, 70)$, and we display those (m_1, m_2)-harmonics of the Melnikov function in the s-strip defined by $\alpha = 1/2 - \eta$ with $\eta = 0.2$. We note that the dominant term of the Melnikov function changes from the $(41, 29)$-harmonic to the $(99, 70)$ in the range of ε of the figure. Moreover, the other harmonic terms inside the s-strip not related to best approximants, have a negligible relative contribution to the total amplitude of the Melnikov function. In particular, the numerical illustrations of the next section also support this fact. Indeed, rigorous bounds for non-best approximant resonant sequences were obtained in [15] for the golden mean in a slightly different context. Based on these observations, we restrict from now on to the sequence of best approximants of ω to analytically describe some properties regarding the asymptotic behaviour of $|M(\theta_0, \psi_0, \varepsilon)|$.

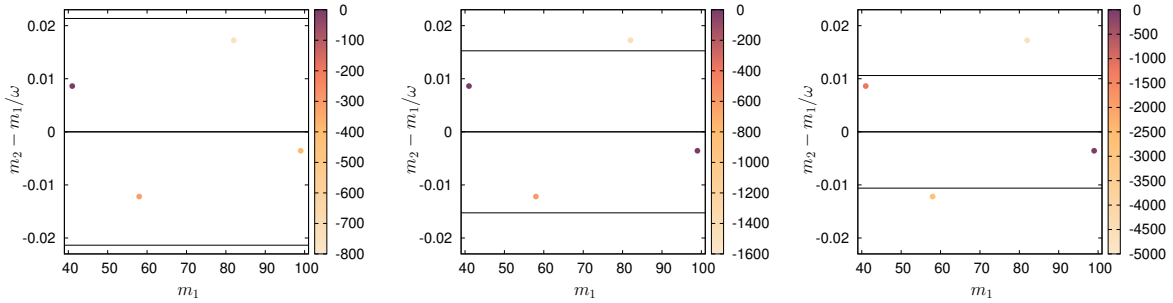

Figure 7: From left to right, we consider $\log \varepsilon = -10, 10.96$ and -12, and we display the (m_1, m_2)-harmonics that lie in the s-strip for $\log \varepsilon = -10$. The horizontal lines delimit the s-strip with $\alpha = 1/2 - \eta$, $\eta = 0.2$. The colour indicates the relative contribution of C_{m_1,m_2} to the total amplitude of the Melnikov function. We observe a change of dominant harmonic between two consecutive best approximants of ω, $(41, 29)$ and $(99, 70)$, while the largest relative amplitude of the non-best approximant harmonics, $(58, 41)$ and $(82, 58)$, is $\mathcal{O}(\exp(-311))$.

4.3 Arithmetic properties of ω: different asymptotic behaviours

The expression (11) of the Melnikov function allows us to investigate the asymptotic behaviour of the splitting. As it is well-known, the details of the asymptotic behaviour are related to the arithmetic properties of ω. This relation was further investigated in [19], below we report similar computations for the Hopf-zero scenario here considered.

As already said, most of the illustrations are performed for the external frequency $\omega = \sqrt{2}$, a noble number whose continuous fraction expansion (CFE) is given by $[1; 2, 2, 2, ...]$. The best approximants of $\sqrt{2}$ are quotients p_n/q_n, $n \geq 1$, where q_n is a Pell number and p_n is a Pell-Lucas number. The recurrence $q_0 = 0$, $q_1 = 1$, $q_n = 2q_{n-1} + q_{n-2}$ give the denominators and the numerator is obtained as $p_n = q_n + q_{n-1}$. Both sequences $(p_n)_{n\geq 1}$ and $(q_n)_{n\geq 1}$ grow as δ_S^n, being $\delta_S = 1 + \sqrt{2}$ the silver ratio.

In Fig.8 one can see the behaviour of the amplitude of the Melnikov function with respect to ε for $\omega = \sqrt{2}$. If, according to (13), one naively expects such behaviour to be exponentially small in ε, the corresponding plot reveals a piece-wise structure with apparently different slopes, see Fig. 8 left. This is related to the fact that, within different ranges of ε, a different combination of the internal and external frequencies defines a fast angle that, however, evolves much slower than the θ, ψ angles (which evolve as $\sim 1/\varepsilon$). In particular, see [20] for example, for constant type irrational numbers, the slowest combination of the two angles defines an angle that generally evolves as $\sim 1/\sqrt{\varepsilon}$, meaning that the splitting is expected to behave exponentially small in $\sqrt{\varepsilon}$. The corresponding representation in agreement with such behaviour shows the sequence of bumps related to the different approximants of ω that define the slowest combination of the angles in each range of ε, see Fig. 8 center.

Note however that in such a figure the bumps are aligned along a curve with a non-zero average slope. Indeed, a numerical fit by a function of the form $a|x|^{1/2} + b$ in the range $[-36.74, -27.69]$ gives $a \approx -1.81564$, see Fig. 8 right. This indicates that a term $|\log \varepsilon|^{1/2}$ must be included in the exponent of the asymptotic behaviour. The reason for this extra logarithmic term is related to the analytic properties of the perturbation: as c is considered to be constant (and equal to $1/2$), the width of the analyticity strip of the factor $f(y) = 1/(c - y)$ of the periodic forcing tends to infinity as $\varepsilon \to 0$. See Section 4.4 for an analytical justification of the behaviour of

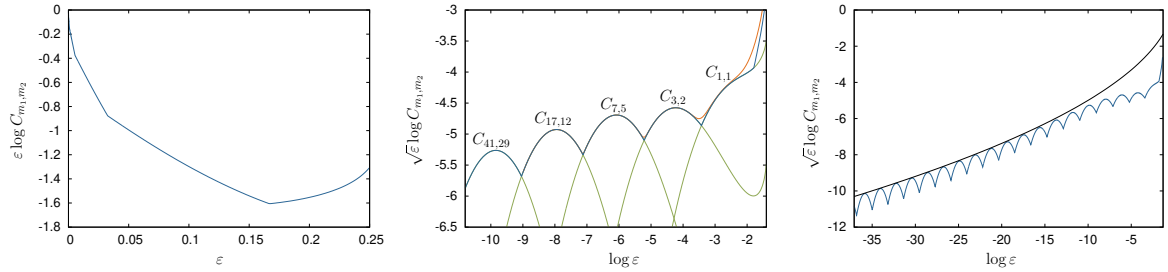

Figure 8: We display the behaviour of $|M(\theta_0, \psi_0, \varepsilon)|$ with respect to ε and $\log \varepsilon$ for $\omega = \sqrt{2}$ in different scales. The contribution of the leading harmonic C_{m_1,m_2} is shown in blue. The sum of all (m_1, m_2) such that the relative contribution of $C_{m_1,m_2} > 10^{-10}$ is shown in orange. Moreover, we display in green the amplitudes C_{m_1,m_2} of the harmonics (m_1, m_2) such that m_1/m_2 is a best approximant of ω.

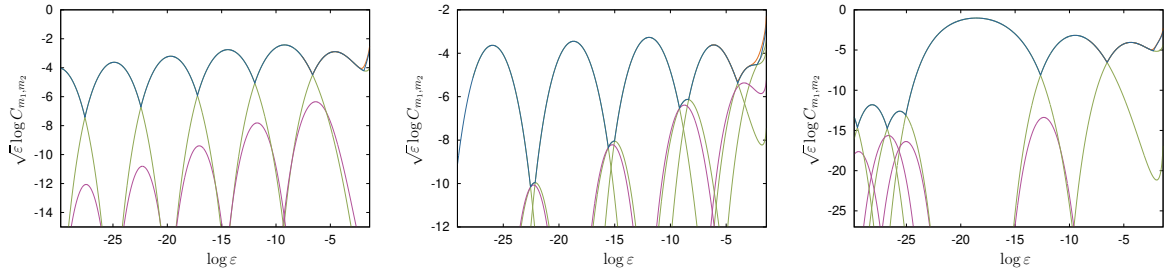

Figure 9: For $\delta = 0.01$, we consider $\omega = \omega_{1,10} = [1, 10, 1, 10, ...]$ (left), $\omega = \sqrt{e}$ (center) and $\omega = \pi$ (right). As in Fig. 8, we show $|M(\theta_0, \psi_0, \varepsilon)|$ and some of the contributions of terms C_{m_1,m_2}, the behaviour of the dominant term/s of the Melnikov function in orange and the leading term in blue. In green (resp. in purple) we display harmonics corresponding to best approximants of ω that become (resp. never become) the leading harmonic in a range of ε.

C_{m_1,m_2} displayed in Fig. 8.

Other possible behaviours of the amplitude are observed for other frequencies $\omega \in \mathbb{R}\backslash\mathbb{Q}$. In Fig. 9 we show, from left to right, the results for $\omega = \omega_{1,10} = [1, 10, 1, 10, ...] \approx 1.091607978$, $\omega = \sqrt{e}$ and $\omega = \pi$. In all cases, one can see that when ε decreases, there are many changes in the dominant harmonic of the Melnikov function. By a *dominant harmonic* (or *dominant harmonics*) of the amplitude of the series of the Melnikov function we refer to a harmonic term (resp. a finite sum of harmonic terms) that is of greater order in ε than the sum of the remaining harmonic terms of the Melnikov function series. Note that the *leading harmonic* term (the harmonic term with the largest amplitude) of the Melnikov function series might not be dominant in the previous sense. In Figs. 8 and 9 the leading harmonic is displayed in blue. In orange, we display the amplitude of the dominant harmonic/s, computed by adding harmonic terms up to a relative contribution to the total amplitude of 10^{-10}. As expected, the leading harmonics are related to the best approximants of the frequency ω. The amplitudes C_{m_1,m_2} of the harmonic term corresponding to (m_1, m_2) where m_1/m_2 is a best approximant of ω are displayed in green if they become dominant within a certain range of ε, and in purple otherwise. We note that the leading term coincides with the dominant term in large ranges of $\log \varepsilon$ (and so the orange line is almost invisible in the plots), but they do not coincide when ε is large and near the changes of leading harmonic, meaning that at least two harmonics are needed to describe the dominant behaviour of the splitting amplitude in the small ranges of ε where a change of the leading harmonic is detected.

For $\omega = \omega_{1,10}$ and $\omega = \sqrt{e}$ there is a sequence of *hidden harmonics*, that is, a sequence of best approximant harmonics that never (for any range of ε) become the leading harmonic of the Melnikov function (in purple in Fig. 9). Concretely, $\omega = \omega_{1,10}$ has a 2-periodic CFE and one in two consecutive best approximants is hidden. For $\omega = \sqrt{e}$ one in three consecutive best approximants harmonics, starting from the 3rd one $(3, 2)$, is hidden. In [19] it was shown that for any $\omega \in \mathbb{R} \setminus \mathbb{Q}$ there are no two consecutive harmonics associated with the best approximants that are hidden. Hidden harmonics are also observed in Fig. 9 right for $\omega = \pi$. There is strong numerical evidence that this is a typical number in a measure theoretical sense and, for such type of numbers, it was conjectured that the distribution of the hidden best approximant harmonics in the set of consecutive best approximant harmonics follows a Gaussian distribution law [19]. Note also that no hidden harmonic are observed for $\omega = \sqrt{2}$ in Fig. 8. The previous illustrations indicate that the details of the asymptotic behaviour of the splitting function strongly depends on the Diophantine properties of ω.

4.4 The amplitude of the leading harmonic

The illustrations in Section 4.3 show that under a quasiperiodic forcing and avoiding the small ranges of $\log \varepsilon$ where the leading harmonic changes, the leading harmonic of the Melnikov function corresponds indeed to the dominant harmonic. This has been proved in similar problems under suitable hypotheses on the perturbation and under specific arithmetic properties of the frequencies involved. A direct proof in this setting for concrete frequency ω seems to be a bit more involved because one of the frequencies involved in the quasi-periodic interaction is already present in the unperturbed dynamics and, hence, the amplitude of the harmonics are defined through series expansions, which might be difficult to handle (see comments in Section 4.2) and Appendix A.

As shown in Section 4.2 and 4.3, a key role is played by the Diophantine properties of ω. Given m_1/m_2 an approximant of ω, let $c_{m_1,m_2} > 0$ be the constant such that

$$s = |m_2\omega - m_1| = \frac{1}{c_{m_1,m_2} m_1}. \tag{14}$$

The constants c_{m_1,m_2} are relevant to describe the relative influence of the consecutive best approximants, and determine if they are dominant in a small range or hidden, see [19, 20]. Below we are mainly interested in harmonics related to best approximants and, if m_1/m_2 is the n-th best approximant of ω, we denote the corresponding constant c_{m_1,m_2} by c_n. The convergence properties of the sequence $\{c_n\}_{n\geq 0}$ depend on the frequency type considered. Concretely, see [20] for proofs, the following properties hold:

1. For a quadratic irrational ω, $\{c_n\}_{n\geq 0}$ is a periodic sequence with the same period that exhibits its CFE. In particular, for constant type frequency ω, $\{c_n\}_{n\geq 0}$ converges.
2. For ω with unbounded CFE, $\{c_n\}_{n\geq 0}$ has a subsequence that diverges to ∞ when $n \to \infty$.

Note that in Section 4.3 we illustrated the behaviour for different CFE. In particular, we considered the quadratic irrational frequency $\omega = \sqrt{2}$ with constant type CFE, $\omega = \omega_{1,10}$ with periodic CFE, $\omega = \sqrt{e}$ which has an unbounded CFE (with quotients $q_{3j+1} = 4j - 3$ and $q_i = 1$ otherwise), and $\omega = \pi$ whose CFE properties are not known (e.g. is the CFE of π bounded?) but do not seem to exhibit any regular pattern.

Denote by $m_{1,n}/m_{2,n}$ the n-th best approximant of ω. Assume that the sequence $(m_{1,n}/m_{2,n})_{n\geq 0}$ of best approximants is the union of a finite number of disjoint subsequences with the property

that, for each subsequence $(m_{1,n_k}/m_{2,n_k})_{k\geq 0}$, there are constants $k_1, k_2 > 0$ and a function ϕ such that

$$k_1\phi(m_{1,n_k})/m_{1,n_k} \leq |m_{2,n_k}\omega - m_{1,n_k}| \leq k_2\phi(m_{1,n_k})/m_{1,n_k},$$

for all $k \geq 1$. From now on we consider Diophantine frequencies ω that verify the previous assumption. In particular, this means, that $c_{n_k}\,\phi(m_{1,n_k})$ tends to constant as n tends to ∞.

Starting from the expression (13) for the amplitude of the (m_1, m_2)-harmonic, we look for $s = s(\varepsilon)$ that describes the behaviour of the leading harmonic. As said, we restrict to those harmonics corresponding to best approximants of ω. First, we study the contribution of $S_A = \sum_{i\geq 0} A_i$ to each term C_{m_1,m_2}. Note that, for ε small enough, $\lim_{i\to\infty} A_{i+1}/A_i = 4\varepsilon^2/c^2 < 1$ and so the leading term of S_A is A_0. To prove that A_0 is indeed the dominant term of the sum, we consider $S_A = A_0\left(1 + \sum_{i\geq 1} A_i/A_0\right)$. Recall that we consider $\varepsilon < s < \varepsilon^\alpha$ (the contribution of the harmonics with $s \leq \varepsilon$ and $s \geq \varepsilon^\alpha$ is of smaller order in ε, see Appendix A) and sm_1 is bounded from above. Then, there is $\tilde{k} \in \mathbb{R}$ such that

$$\frac{A_i}{A_{i-1}} \leq \frac{1}{c^2}\left[\frac{s}{m_1} + \varepsilon^2(m_1+4)\right] < \tilde{k}\varepsilon^\alpha,$$

and, provided ε small enough, there exists $\tilde{K}$ such that $\frac{A_i}{A_{i-1}} < \tilde{K}\varepsilon^\alpha < 1$ for all $i \geq 1$ so that

$$\sum_{i\geq 1} A_i/A_0 = \sum_{i\geq 1} \frac{A_i}{A_{i-1}}\frac{A_{i-1}}{A_{i-2}}\cdots\frac{A_1}{A_0} < \sum_{i\geq 1}(\tilde{K}\varepsilon^\alpha)^i = \frac{\tilde{K}\varepsilon^\alpha}{1-\tilde{K}\varepsilon^\alpha}.$$

Thus we can approximate the amplitude of the harmonics as

$$C_{m_1,m_2} \approx \frac{2^6\pi}{\sqrt{d^2-1}}\frac{\varrho_d^{m_2}}{c^{m_1}(m_1+4)!}P_{m_1+4}(s,\varepsilon)\exp\left(\frac{-s\pi}{2\varepsilon}\right)(1+O(\varepsilon^\alpha)).$$

Moreover, since the leading harmonic corresponds to $s > \varepsilon$, Lemma A.1 implies that $P_{m_1+4}(s,\varepsilon) \leq (s^2+\varepsilon^2(m_1+4)^2)^{\lfloor\frac{m_1+4}{2}\rfloor}$. Using Stirling approximation, if m_1 is large enough, one has $\frac{1}{(m_1+4)!} \approx \sqrt{2\pi}e^{m_1+4}(m_1+4)^{-m_1-9/2}$, and we obtain

$$C_{m_1,m_2} \approx \frac{2^6\pi}{\sqrt{2\pi(d^2-1)}}\frac{\varrho_d^{m_2}e^{m_1+4}}{c^{m_1}(m_1+4)^{m_1+9/2}}(s^2+\varepsilon^2(m_1+4)^2)^{\lfloor\frac{m_1+4}{2}\rfloor}\exp\left(\frac{-s\pi}{2\varepsilon}\right). \tag{15}$$

The error from Lemma A.1, see Remark A.1, makes $\frac{\varepsilon}{s}\log C_{m_1,m_2}$ to have an error of order $\frac{\varepsilon^3}{3\ell^3 s^6} + \frac{\varepsilon}{2s}\log(1+\varepsilon^2/(\ell^2 s^4))$ when using the previous approximation.

4.4.1 The amplitude of the leading harmonic for constant type ω

We first consider a constant type frequency ω and let $\ell = \lim_{n\to\infty} c_n$. Thus, we can approximate $m_1 \approx \frac{1}{\ell s}$, $m_2 \approx \frac{1}{\omega\ell s}$, which means that (15) is approximated as

$$C_{m_1,m_2} \approx K\sqrt{\ell s}\left((\ell^2 s^4 + \varepsilon^2(1+4\ell s)^2)^{1/2}\varrho_d^{1/\omega}c^{-1}e\right)^{\frac{1}{\ell s}}\exp\left(\frac{-s\pi}{2\varepsilon}\right), \tag{16}$$

for some constant $K > 0$.

Given $\varepsilon > 0$, the leading harmonic corresponds to $s = s(\varepsilon)$ that gives the maximum value of C_{m_1,m_2}. Then $s = s(\varepsilon)$ is a solution of the equation $\ell s^2 \frac{\partial}{\partial s} \log C_{m_1,m_2} = 0$, which reads

$$\frac{\ell s}{2} - \log\left(\left(\ell^2 s^4 + \varepsilon^2(1+4\ell s)^2\right)^{1/2} \varrho_d^{1/\omega} c^{-1} e\right) + 2\left(\frac{\ell^2 s^4 + 2\ell s\varepsilon^2(1+4\ell s)}{\ell^2 s^4 + \varepsilon^2(1+4\ell s)^2}\right) = \ell s^2 \frac{\pi}{2\varepsilon}. \tag{17}$$

Write the lefthand part of the previous equation as $L_1(s,\varepsilon) + 2L_2(s,\varepsilon)$ and let $\eta = \ell\varepsilon^2\,(\ell^2 s^4 + \varepsilon^2)^{-1}$. For $s > \varepsilon$ one has

$$\begin{aligned} L_1(s,\varepsilon) &= \frac{\ell s}{2} - \log\left(\left(\ell^2 s^4 + \varepsilon^2(1+4\ell s)^2\right)^{1/2} \varrho_d^{1/\omega} c^{-1} e\right) \\ &= -\frac{1}{2}\log(\ell^2 s^4 + \varepsilon^2) - \log(\rho_d^{1/\omega} c^{-1} e) + \mathcal{O}\left(s, \eta s\right), \\ L_2(s,\varepsilon) &= \frac{\ell^2 s^4 + 2\ell s\varepsilon^2(1+4\ell s)}{\ell^2 s^4 + \varepsilon^2(1+4\ell s)^2} = 1 - \frac{\varepsilon^2}{\ell^2 s^4 + \varepsilon^2} + \mathcal{O}\left(\eta s, \eta^2 s\right), \end{aligned} \tag{18}$$

where we made explicit the term that depends on the constants c and d, related to the width of the analytic strips of the perturbation, in the expansion of L_1. If, as we have assumed through the manuscript, one considers c and d as constants, then such a term in the expansion of L_1 is $\mathcal{O}(1)$ and the equation (17) reduces to

$$\varepsilon \log(\zeta^2 + \varepsilon^2) - \pi\zeta + \mathcal{O}\left(\varepsilon, \eta\varepsilon\right) = 0, \tag{19}$$

where $\zeta = \ell s^2$. We look for a solution $\zeta(\varepsilon) = \zeta_0(\varepsilon) + \zeta_1(\varepsilon)$ where $\zeta_0(\varepsilon)$ is the solution of equation (19) ignoring the $\mathcal{O}(\varepsilon, \eta\varepsilon)$-terms. One has

$$\zeta_0(\varepsilon) = \frac{2}{\pi}\,\varepsilon|\log\varepsilon| + \mathcal{O}\left(\varepsilon \log|\log\varepsilon|\right). \tag{20}$$

Note that this implies that $\eta = \ell\varepsilon^2(\zeta_0^2(\varepsilon) + \varepsilon^2)^{-1} \sim |\log\varepsilon|^{-2} \ll 1$ and hence the previously ignored terms are $\mathcal{O}(\varepsilon)$. One checks that these ignored terms in equation (19) produce a correction $\mathcal{O}(\varepsilon)$ to $\zeta_0(\varepsilon)$, which is smaller than the error in (20), and we conclude that $\zeta(\varepsilon) \approx \zeta_0(\varepsilon)$ and

$$s(\varepsilon) = \sqrt{\frac{2\varepsilon|\log\varepsilon|}{\ell\pi}} + \mathcal{O}\left(\sqrt{\varepsilon}\,\frac{\log|\log\varepsilon|}{\sqrt{|\log\varepsilon|}}\right). \tag{21}$$

Therefore, as one obtains by substituting $s(\varepsilon)$ into (16), the expected behaviour of the amplitude of the Melnikov function is of the form

$$\log C_{m_1,m_2} \approx -\sqrt{\frac{2\pi|\log\varepsilon|}{\ell\varepsilon}}, \tag{22}$$

in those ranges of ε where the leading harmonic becomes dominant.

We remark that the behaviour (22) is consistent with the exponentially small remainder obtained after performing the optimal number of steps of averaging to remove the time dependence of the fast quasiperiodic perturbation in (8), see [39]. As pointed out in [39, 16], the extra logarithmic term in the exponent appears as a consequence of the factorial decay of the Fourier coefficients, see Remark 4.2, because $f(y)$ behaves as an entire function as $\varepsilon \to 0$ since $\rho_\theta = \operatorname{arcsinh}(c/\sqrt{\nu}\varepsilon)$. Note that such factorial decay of the prefactor is compensated with the exponential decay in ε of the exponential part when solving equation (17). This logarithmic term justifies the behaviour of the amplitude observed in Fig. 8 for $\omega = \sqrt{2}$.

Remark 4.2. Let $f(z) = \sum_{k\in\mathbb{Z}} c_k e^{ikz}$ be the Fourier series representation of a 2π-periodic function f. If f is analytic in the strip $\{z \in \mathbb{C}, |\mathrm{Im} z| < \rho\}$ then a standard application of the Cauchy theorem shows that $|c_k| = \mathcal{O}(\exp(-|k|r))$ for $0 < r < \rho$. If instead f is entire then one has freedom in choosing the width of the strip of the domain of analyticity and, in particular, one can choose ρ depending on k before applying Cauchy theorem. Taking $\rho(k) \sim \log(k)$ then it follows from the Stirling approximation that $|c_k| = \mathcal{O}(1/k!)$. Any log-type growth of ρ as a function of k leads to a factorial decay (with different constants) of the Fourier coefficients of an entire function f.

4.4.2 The amplitude of the leading harmonic for ω with unbounded regular CFE

We consider $\omega = \sqrt{e}$. The bounded partial subsequences $\{c_{q(n)}\}_{n\geq 0}$ of $\{c_n\}_{n\geq 0}$ converge to $\ell \approx 2/\sqrt{e}$. Then one expects $\sqrt{\varepsilon}|\log\varepsilon|^{-1/2}\log C_{m_1,m_2} \approx -2.276$ as given by (22). On the other hand, numerical computations of the unbounded subsequence $\{c_{3n}\}_n$ seem to indicate that $\omega = \sqrt{e}$ verifies that $|q\omega - p| \geq K\phi(q)/q$ with $\phi(q) = \log(\log(q))/\log(q)$ for all $p, q \in \mathbb{Z}\setminus\{0\}$. In other words, if $m_{1,n}/m_{2,n}$ denotes the n-th best approximant of ω, then $s = |m_{2,3n}\omega - m_{1,3n}| \approx \tilde{k}\phi(m_{1,3n})/m_{1,3n}$. Hence, let $\tilde{\ell} = \lim_{n\to\infty} c_{3n}\,\phi(m_{1,3n})$ and $s \approx \phi(m_{1,3n})/(\tilde{\ell} m_{1,3n})$. By substitution into (15), one obtains

$$C_{m_1,m_2} \approx \left(\rho_d^{1/\omega} e\, c^{-1}\right)^{m_1} \left(\frac{(\phi(m_1))^2}{\tilde{\ell}^2\, m_1^4} + \varepsilon^2\right)^{\frac{m_1}{2}} \exp\left(-\frac{\phi(m_1)\pi}{2\tilde{\ell} m_1 \varepsilon}\right),$$

where $m_1 = m_{1,3n}$, $m_2 = m_{2,3n}$ and we have ignored some constants and simplify some terms that do not affect the exponent of C_{m_1,m_2}. Note that $\zeta = s/m_1 = \phi(m_1)/(\tilde{\ell} m_1^2)$ verifies the equation (19) and, hence, $\zeta \approx \frac{2}{\pi}\varepsilon|\log\varepsilon|$. This implies

$$m_1 = m_{1,3n} \approx \frac{\sqrt{\pi \log|\log\varepsilon|}}{\sqrt{\tilde{\ell}\varepsilon}|\log\varepsilon|}\,(1 + o(1))\,,$$

and substituting it in the expression of C_{m_1,m_2} above one has

$$\log C_{m_1,m_2} \approx -2\sqrt{\frac{\pi \log|\log\varepsilon|}{\tilde{\ell}\,\varepsilon}}\,(1 + o(1)).$$

This justifies the observed behaviour of the maxima of the blue curves in Fig. 9 center.

4.4.3 The amplitude of the leading harmonic in the non-entire analytic case

Next, we consider what happens when the analytic function f in the perturbation no longer behaves as an entire function as $\varepsilon \to 0$. To this end, let $c = C\varepsilon$, hence the width of the strip is $\rho_\theta = \mathrm{arcsinh}(C/\sqrt{\nu})$. In such a case all the explicit terms (18) are $\mathcal{O}(1)$. Ignoring $\mathcal{O}(\eta s, \eta^2 s)$-terms, we look for $s(\varepsilon) = A\sqrt{\varepsilon}$ such that is a solution of

$$-\frac{1}{2}\log(\ell^2 s^4 + \varepsilon^2) - \log\frac{K_0}{\varepsilon} + 2 - 2\frac{\varepsilon^2}{\ell^2 s^4 + \varepsilon^2} = \frac{\ell\pi s^2}{2\varepsilon},$$

where $K_0 = \rho_d^{1/\omega} C^{-1} e$. Introducing $z = \ell^2 A^4 + 1$ and denoting $\tilde{K}_0 = 4 - 2\log K_0$, the last equation reduces to

$$\pi z\sqrt{z-1} + z\log z + 4 = \tilde{K}_0 z,$$

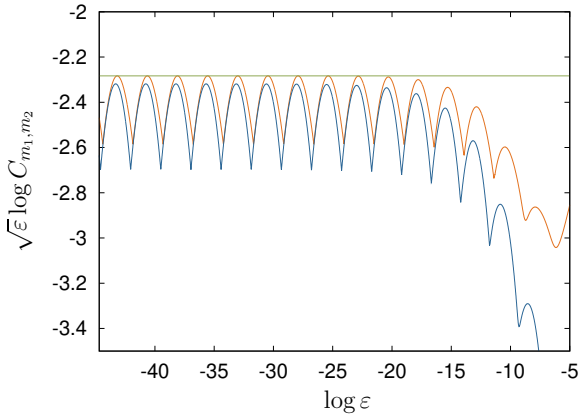

Figure 10: We display in blue the behaviour of $|M(\theta_0, \psi_0, \varepsilon)|$ when $\omega = \sqrt{2}$ and $c = 5\varepsilon$. The approximation of C_{m_1,m_2} defined in (15) is shown in orange so that one can see the asymptotic behaviour predicted in (23) and the error of using such approximation.

which admits a unique solution z_* for any $\tilde{K}_0 \geq 4$. This implies that $s(\varepsilon) = \mathcal{O}(\sqrt{\varepsilon})$. Then the ignored terms in the equation above for z are $\mathcal{O}(\sqrt{\varepsilon})$ and they do not affect the obtained estimate of $s(\varepsilon)$. Substituting $s(\varepsilon) = A\sqrt{\varepsilon}$ into (16) one obtains

$$\log C_{m_1,m_2} \approx \frac{-\beta}{\sqrt{\varepsilon}}, \quad \text{where} \quad \beta = \frac{A\pi}{2} - \frac{1}{A\ell}\log(K_0\sqrt{1+\ell^2A^4}). \tag{23}$$

As an example, for $\omega = \sqrt{2}$, taking $C = 5$, $d = 5$, one has $\tilde{K}_0 \approx 8.46086$, $z_* \approx 4.7227$, $A \approx 0.9822$ and $\beta = 2.28313$, since $\ell = 2$,.

The error of using approximation (15) implies that, instead of the behaviour predicted by (23), one expects the amplitude of the leading term of the Melnikov function to behave as [2]

$$\sqrt{\varepsilon}\log C_{m_1,m_2} \approx -\beta + \arctan\left(\frac{1}{\ell A^2}\right) - \frac{1}{\ell A^2} + \mathcal{O}(\sqrt{\varepsilon}).$$

This difference is shown in Fig. 10. Note that this error is $\mathcal{O}(|\log\varepsilon|^{-3})$ when $f(y)$ behaves as an entire function, hence does not change the behaviour of the amplitude given by (22).

4.5 Rational approximations to ω

Let us comment now on the asymptotic behaviour of the amplitude when one considers $\omega = \omega_{\mathbb{Q}} = p/q \in \mathbb{Q}$. In this case, the periods of the internal and external frequency are commensurable and the system can be expressed as a periodic perturbation of a planar system. Hence the behaviour of the splitting function differs from that explained for $\omega \in \mathbb{R} \setminus \mathbb{Q}$. This is indeed a consequence of the well-known fact that a rational number is badly approximated by other rationals:

Lemma 4.1 ([8, 28])**.** *The distance between $\omega_{\mathbb{Q}} = p/q$ and any $\tilde{\omega}_{\mathbb{Q}} = m/n \in \mathbb{Q}$, both assumed to be reduced rationals, is bounded from below as $|\tilde{\omega}_{\mathbb{Q}} - \omega_{\mathbb{Q}}| \geq \frac{1}{qn}$, and the equality holds if there is $k \in \mathbb{Z}$ such that $m = kp + m_0$, $n = kq + n_0$ and m_0, n_0 are such that $|pn_0 - qm_0| = 1$.*

[2] For constant type ω and assuming the decay of the Fourier coefficients of the perturbation given by a finite strip of analyticity, the upper bound in [39] has an extra factor $|\log\varepsilon|^{-1/2}$. This is a consequence of the lemma bounding the contribution of the small divisors, see [38]. However, our results seem to indicate that the splitting behaviour in this case does not have such a logarithmic term.

Then, given $\omega_{\mathbb{Q}} = p/q$, the set $\Gamma = \{(m_1, m_2) \in \mathbb{Z}^2, pm_2 - qm_1 = 1\} \subset \mathbb{Z}^2$ is a one dimensional sublattice generated by the vector (p, q). For any pair $(m_1, m_2) \in \Gamma$ one has $s = |m_2 \frac{p}{q} - m_1| = \frac{1}{q}$. The amplitude of the corresponding (m_1, m_2)-harmonic of the Fourier expansion of the Melnikov function is then

$$C_{m_1,m_2} \sim \exp\left(\frac{-\pi}{2q\varepsilon}\right).$$

Remark 4.3. The behaviour of the amplitude when considering a rational frequency resembles that of an autonomous perturbation of X_0. Autonomous analytic conservative perturbations have been extensively studied in the literature. In general, the rotational symmetry of X_0 is broken due to the perturbation and then the invariant manifolds show an exponentially small splitting [17]. As a particular example, one can consider X_1 with $g(\psi) \equiv 1$. This is a regular perturbation for which it was proved in [1] that the Melnikov function gives the first order of the asymptotic behaviour of the splitting. Thus, computing the Melnikov function as a simpler version of the one in Section 4.1 one gets

$$M(\theta_0, \varepsilon) = \sum_{m \geq 1} \hat{C}_m T(m\theta_0),$$

where $T(\alpha) = \cos(\alpha)$ if m is odd and $T(\alpha) = \sin(\alpha)$ otherwise. The amplitude of $M(\theta_0, \varepsilon)$ is given by

$$|\hat{C}_m| = \frac{2^5\pi}{c^m} \exp\left(\frac{-m\pi}{2\varepsilon}\right) \sum_{i \geq 0} \frac{(m+2i)!}{c^{2i}(m+i)!(m+2i+4)!i!} P_{m+2i+4}(m),$$

where $P_p(m) = (m^2 + \varepsilon^2(p-2)^2)P_{p-2}(m)$, $P_0 = 1, P_1 = m$. Therefore, considering just the contribution of the leading harmonic, which is given by $m = 1$, we conclude that the behaviour of the Melnikov function becomes exponentially small as $\varepsilon \searrow 0$. The difference to the rational frequency perturbation previously considered is that, in the last, all pairs $(m_1, m_2) \in \Gamma$ contribute with the same exponential part to the amplitude of the splitting.

A situation of particular interest is to consider the rational frequency $\omega_{\mathbb{Q}} = p_n/q_n$ to be the n-th best approximant of an irrational frequency ω. Then, Lemma 4.1 tells us that, for ε small enough, the leading harmonics (m_1, m_2) of the Melnikov function of $\omega_{\mathbb{Q}}$ are $(m_1, m_2) = (kp_n + p_{n-1}, kq_n + q_{n-1})$, for any $k \in \mathbb{Z}$, the amplitude of all of them having the same exponentially small part in ε. On the other hand, the analytic properties of the perturbation guarantee (at least, see 4.2) an exponential decay of the prefactor term with respect to the total order of the harmonics. Consequently, the harmonic (p_{n-1}, q_{n-1}) is expected to give the largest contribution to the amplitude of the Melnikov function for $\omega_{\mathbb{Q}}$ corresponding to the n-th best approximant. In Fig.11 one can see the behaviour of the amplitude of the Melnikov function with respect to ε for one best approximants $\omega_{\mathbb{Q}}$ of $\omega = \sqrt{2}$. We see that, when $\varepsilon \to 0$, the largest contribution to the amplitude C_{m_1,m_2} corresponds to the best approximant m_1/m_2 prior to $\omega_{\mathbb{Q}}$ of ω.

It is also of interest to illustrate the behaviour of the amplitude when perturbing the frequency from the approximant $\omega_{\mathbb{Q}}$ of ω. The Fig. 12 left shows this behaviour for some intermediate frequencies $\tilde{\omega} = 7/5 + \nu$ between $\omega_{\mathbb{Q}} = 7/5$ and $\omega = \sqrt{2}$. Concretely, we show the amplitude for values of ν equal to $\nu_1 = 10^{-50}$, $\nu_2 = 10^{-47}$, $\nu_3 = 10^{-18}$, $\nu_4 = 10^{-5}$, $\nu_5 = 6 \times 10^{-3}$ and $\nu_6 = 10^{-2}$. Note that:

- For any frequency $\tilde{\omega}$ with $\omega_{\mathbb{Q}} < \tilde{\omega} < \omega$, the largest contribution to the amplitude of the splitting when $\varepsilon \to 0$ is no longer given by the $(3, 2)$-harmonic (as, on the contrary, happens for $\omega_{\mathbb{Q}} = 7/5$ since $3/2$ is the best approximant of $\sqrt{2}$ prior to $7/5$). In particular, for the frequencies considered in the plot, there is a range $(\varepsilon_1^j, \varepsilon_2^j)$ of values of ε for which the largest contribution to the amplitude is given by the $(7, 5)$-harmonic itself.

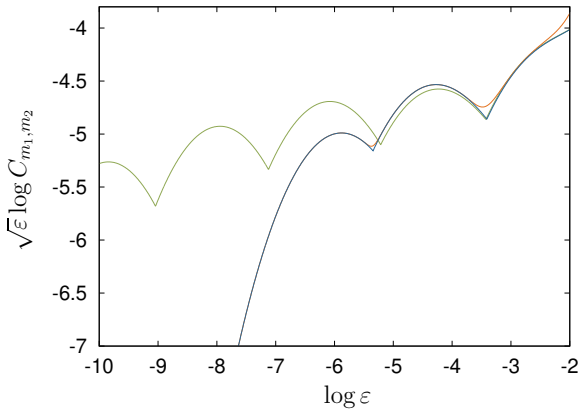

Figure 11: Behaviour of $|M(\theta_0,\psi_0,\varepsilon)|$ when $\delta = 0.01$ and $\omega_{\mathbb{Q}} = 17/12$, which is the 4th best approximant of $\omega = \sqrt{2}$. In orange, we display the sum of the amplitude of all the (m_1,m_2)-harmonics of the Melnikov function (with $|m_1|,|m_2| \leq 100$). The orange line is almost coincident with the blue line, which displays the amplitude of the harmonic giving the largest contribution to $|M(\theta_0,\psi_0,\varepsilon)|$. For reference, in green we display the amplitude of the harmonics of the Melnikov function for $\omega = \sqrt{2}$.

- For $\nu = \tilde{\omega} - \omega_{\mathbb{Q}}$ small, the range $(\varepsilon_1,\varepsilon_2)$ where the $(7,5)$-harmonic gives the largest contribution to the amplitude of the splitting is located far away to the left in the plot. Concretely, $\varepsilon_2 \to 0$ as $\nu \to 0$. Accordingly, if $\varepsilon_0 = 2^{-9}$ we show in the plot that for ν_1 one has $\varepsilon_2^1 < \varepsilon_0$, while $\varepsilon_2^j > \varepsilon_0$ for all the other values $j \geq 2$.
- Given ε_0, there is a frequency $\tilde{\omega}^0$ such that, for any frequency with $\tilde{\omega}^0 < \tilde{\omega} < \omega$, the amplitude of the (m_1,m_2)-harmonic for $\tilde{\omega}$ is larger than the amplitude of the (m_1,m_2)-harmonic for ω. In the figure, we show this for $\varepsilon_0 = 2^{-9}$: for frequencies $\tilde{\omega}$ such that $7/5 + \nu_4 \approx \tilde{\omega}^0 < \tilde{\omega} < \omega$, the amplitude of the $(7,5)$-harmonic (the leading one) is larger than the amplitude of the same harmonic for $\omega = \sqrt{2}$.

In order to clarify the previous points, we fix $\varepsilon = \varepsilon_0 = 2^{-9}$ and compute the amplitude C_{m_1,m_2} of the leading harmonic for frequencies of the form $\tilde{\omega} = 7/5 + \nu$. The results are displayed in Fig. 12 right. For this value of ε the leading harmonic of the Melnikov function for $\omega = \sqrt{2}$ is $(7,5)$, as shown in Fig. 11. The platform observed for $\log\nu \lesssim -111$ reflects that the leading harmonic is $(3,2)$ instead. For larger values of ν the $(7,5)$ harmonic becomes the leading one and its contribution to the total amplitude increases linearly in $\log\nu$ until reaching a maximum around $\log\nu \approx -6.65$. After the maximum, the contribution of the $(7,5)$-harmonic to the total amplitude decreases and converges to the contribution of such a leading harmonic that it is observed for $\omega = \sqrt{2}$.

5 Non-transversal heteroclinic orbits when $\varepsilon \to 0$

In $\{z = 0\}$, the values of (θ_0,ψ_0) that correspond to heteroclinic orbits can be determined by the nodal lines of the splitting function. The topology of the nodal lines changes when the dominant harmonic of the splitting function changes. Such bifurcations are related to quadratic tangencies between the 2D invariant manifolds, that will be studied in this section. In Fig. 13 we display two different projections of the invariant manifolds showing one of these bifurcations.

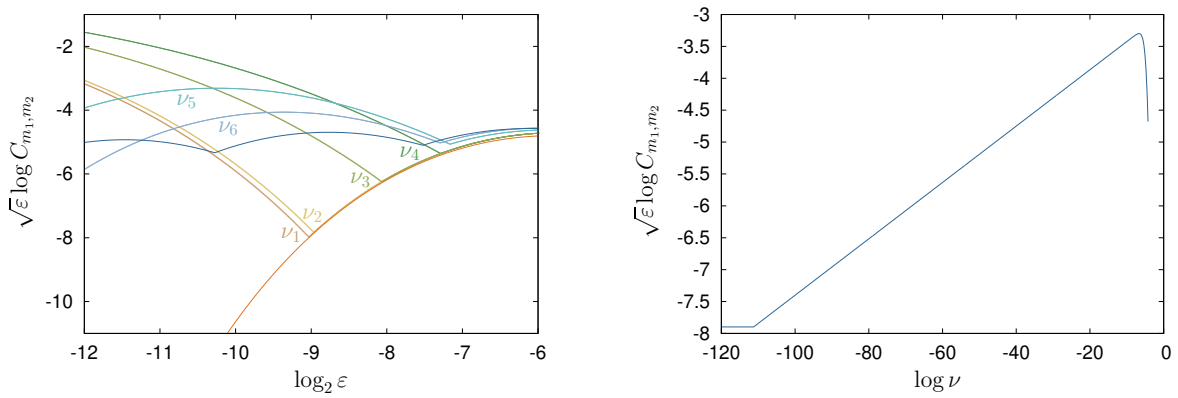

Figure 12: Amplitude of the leading harmonic of the Melnikov function. Left: The amplitude as a function of ε for different frequencies of the form $\tilde{\omega} = 7/5 + \nu_j$, $j = 1, ..., 6$, detailed in the text. For reference also the amplitude of the leading harmonic for $\omega_{\mathbb{Q}} = 7/5$ and $\omega = \sqrt{2}$ are displayed. Right: For $\varepsilon_0 = 2^{-9}$ we consider frequencies $\tilde{\omega} = 7/5 + \nu$ and we represent the amplitude of the leading harmonic as a function of $\log \nu$.

Given $\delta > 0$, we consider the splitting function $S_\delta(\theta_0, \psi_0, \varepsilon) = \delta M(\theta_0, \psi_0, \varepsilon) + \mathcal{O}(\delta^2)$ in (10) and, for $\varepsilon > 0$, we approximate the set of zeros of the splitting function (the nodal lines) by the set $\{(\theta_0, \psi_0) : M(\theta_0, \psi_0, \varepsilon) = 0\} \subset \mathbb{T}^2$. As explained in Section 3, it corresponds to a continuum of heteroclinic orbits between p_- and p_+ lying at the intersection of the 2D stable and unstable invariant manifolds.

Let M_k be the approximation of the Melnikov function obtained as the sum of the k-harmonics of the largest amplitude among the harmonics that correspond to the best approximants of ω. Given $\varepsilon > 0$ we write $M_k \cong M$ if M_k is a dominant approximation of M. Note that the best approximants involved in M_k might not be consecutive best approximants, as there might be some hidden harmonics related to the best approximants for specific frequencies ω.

We assume below that there is $\varepsilon_0 > 0$ such that, for $\varepsilon < \varepsilon_0$ the number of dominant harmonics of the Melnikov function is either one or two. This assumption holds for constant type ω, as we illustrated for $\omega = \sqrt{2}$ in Fig. 8, but it may not hold for other frequency types. For example, for $\omega = \sqrt{e}$, the results in Fig. 14 indicate that at least three dominant harmonics of the Melnikov function are needed in a range of ε where a change of the leading harmonic takes place and, as we can see in Fig. 9 left, one of the dominant harmonics is actually hidden.

Let $\omega \in \mathbb{R} \setminus \mathbb{Q}$ be a Diophantine frequency and assume that, for any $\varepsilon_0 > 0$, there is a numerable number of intervals of $\varepsilon < \varepsilon_0$ for which M_1 is a dominant approximation of M. Denote by (m_1, m_2) the harmonic that defines M_1 in one of these interval ranges of ε, that is,

$$M(\theta_0, \psi_0, \varepsilon) \cong M_1(\theta_0, \psi_0, \varepsilon) = \hat{C}_{m_1,m_2}(\varepsilon) T(m_1\theta_0 + m_2\psi_0),$$

where T is either a cos or sin function depending on the parity of m_1, see (11). Then, the set $\{M_1 = 0\}$ is the intersection of $\mathbb{T}^2$ with the set of parallel lines obtained as vertical translations of $m_2\psi_0 = -m_1\theta_0 + p_0$ by $j \pm \pi/m_2$, where $j \in \mathbb{Z}$ and p_0 is either $\pi/2$ or 0, depending on the parity of m_1 and $g(\psi)$.

Let m_1/m_2 and n_1/n_2 be two consecutive best approximants of ω, and consider an ε-interval around ε_*, where the change of the leading harmonic takes place and the approximation

$$M(\theta_0, \psi_0, \varepsilon) \cong M_2(\theta_0, \psi_0, \varepsilon) = \hat{C}_{m_1,m_2}(\varepsilon) T_1(m_1\theta_0 + m_2\psi_0) + \hat{C}_{n_1,n_2}(\varepsilon) T_2(n_1\theta_0 + n_2\psi_0),$$

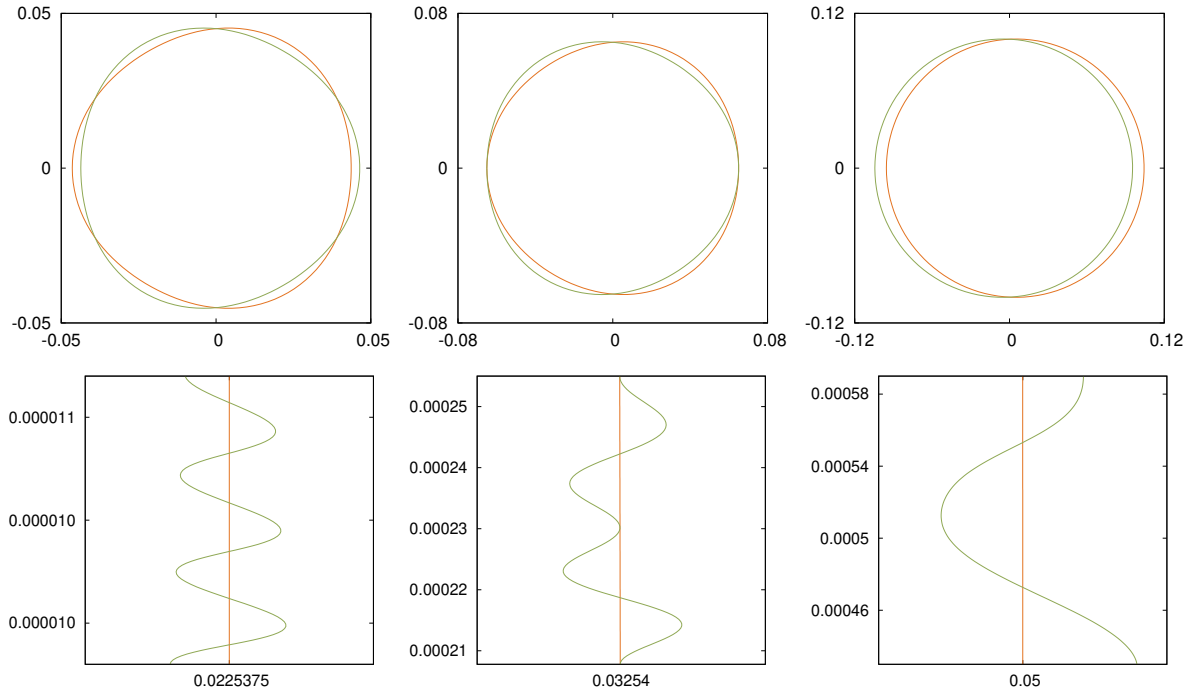

Figure 13: For $\log\varepsilon = -3.79257, \log\varepsilon_* = -3.42536$, and $\log\varepsilon = -2.99573$, we display the (x, y) and (z, x) projections of the invariant manifolds in $\{z = 0\}$ and $\{y = 0\}$, respectively, for $\psi_0 = \pi$ (the relative distance in the first row is magnified by a suitable factor).

is dominant. The functions T_1 and T_2 in M_2 are either cos or sin functions depending on the parity of m_1 and n_1, see (11). In this range, $|\hat{C}_{m_1,m_2}(\varepsilon)|$ is monotonically increasing while $|\hat{C}_{n_1,n_2}(\varepsilon)|$ is decreasing. Let A be the unimodular matrix of the change $\alpha = m_1\theta_0 + m_2\psi_0$, $\beta = n_1\theta_0 + n_2\psi_0$. Then $\tilde{M}_2 = M_2 \circ A$ is given by $\tilde{M}_2(\alpha, \beta) = \hat{C}_{m_1,m_2}(\varepsilon)T_1(\alpha) + \hat{C}_{n_1,n_2}(\varepsilon)T_2(\beta)$. We look for critical saddle points of $\tilde{M}_2$ within the level set $\tilde{M}_2 = 0$. Since $\nabla\tilde{M}_2(\alpha, \beta) = (\hat{C}_{m_1,m_2}(\varepsilon)T_1'(\alpha), \hat{C}_{n_1,n_2}(\varepsilon)T_2'(\beta))$, those critical points are (α_*, β_*) where α_* is a maximum/minimum of $\hat{C}_{m_1,m_2}(\varepsilon)T_1(\alpha)$ and β_* is a minimum/maximum of $\hat{C}_{n_1,n_2}(\varepsilon)T_2(\beta)$. Then the condition $\tilde{M}_2(\alpha_*, \beta_*) = 0$ requires $|\hat{C}_{m_1,m_2}(\varepsilon)| = |\hat{C}_{n_1,n_2}(\varepsilon)|$, which holds for $\varepsilon = \varepsilon_*$. As the determinant of the Hessian matrix is ± 1 the saddle critical points are non-degenerate. This shows that, for ε_*, where the change of leading harmonic takes place, there are two quadratic tangencies between the invariant 2D manifolds $W^u(p_-)$ and $W^s(p_+)$.

In Fig. 15 we illustrate the zero level set of M_2 for values $-3.42505 \le \log\varepsilon \le -3.42844$. The leading harmonic changes from $(1, 1)$ to $(3, 2)$ at $\log\varepsilon_* \approx -3.42536$. Note that, from (12), it follows that $\text{sign}(\hat{C}_{m_1,m_2}) = (-1)^{\lfloor\frac{m_1+3}{2}\rfloor}\,\text{sign}(m_2\omega - m_1)$. Accordingly, one has $\hat{C}_{1,1}(\varepsilon)\hat{C}_{3,2}(\varepsilon) > 0$ and then the two saddle critical points are located at (π, π) and $(0, \pi)$. In Fig. 16 we display the difference between the 2D invariant manifolds around the point $(\theta_0, \psi_0) = (\pi, \pi)$, corresponding to a quadratic tangency. On the other hand, at the next change of leading harmonic one has $\hat{C}_{3,2}(\varepsilon)\hat{C}_{7,5}(\varepsilon) < 0$ and the critical saddle points appear at $(0, 0)$ and $(\pi, 0)$ instead.

The previous considerations lead to the existence of a sequence of values of $\varepsilon > 0$ for which the system (1) has quadratic tangencies of saddle type. Let us state a proper result for a general system of the type considered in this work.

Let $\mathcal{U}_X$ be the class of analytic systems of the form $X = X_0 + \delta X_1$, where:

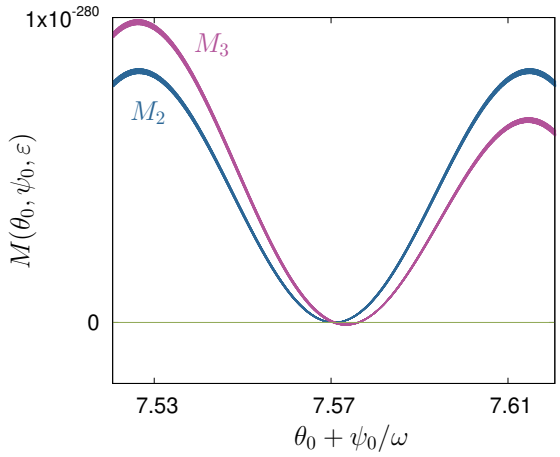

Figure 14: For $\omega = \sqrt{e}$ and for $\log \varepsilon \approx -9.1869$, where there is a change in the leading harmonic, we display in purple the approximation M_3 of the Melnikov function and, in blue, the approximation M_2. The difference between the curves shows that the third harmonic, although hidden, must be included in the dominant terms of the Melnikov function.

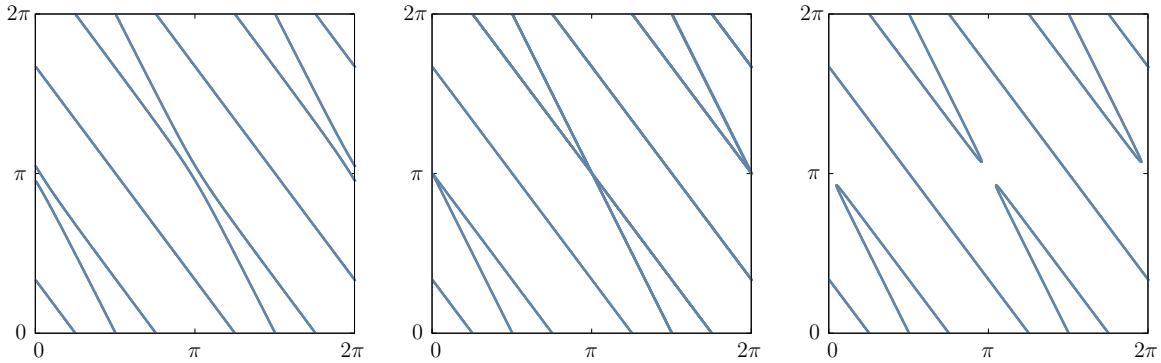

Figure 15: For $\omega = \sqrt{2}$, in the (θ_0, ψ_0)-plane we display the set $\{M_2 = 0\}$ for $\log \varepsilon = -3.42505, -3.42536$ and -3.42844.

(A1) X_0 is a truncation of the conservative 3D Hopf-zero normal form, depending on the parameter ε, up to order ≥ 2. In particular, X_0 commutes with the generator L_z of the rotational symmetry group which defines an internal frequency ω_1 and, for $\varepsilon > 0$, has an integrable bubble of stability bounded by the 2D invariant manifolds of the hyperbolic saddle-foci points. Let $\theta \in [0, 2\pi)$ be the turning angle around the symmetry axis that leaves X_0 invariant.

(A2) X_1 is a perturbation defined by the product of two functions f and g, such that:

- (a) The function f depends on (x, y, z) and has a null 2-jet at the origin. When evaluated on the unperturbed heteroclinic trajectories of the 2D invariant manifolds of the saddle-foci, it depends periodically on $\theta = \omega_1 t + \theta_0 \in [0, 2\pi)$.
- (b) The function g is periodic in $\psi = \omega_2 t + \psi_0 \in [0, 2\pi)$.
- (c) The ratio $\omega = \omega_2/\omega_1$ is Diophantine with bounded CFE.

(A3) The Fourier spectrum is "full" and the decay of the amplitude of the Fourier coefficients is "generic". That is

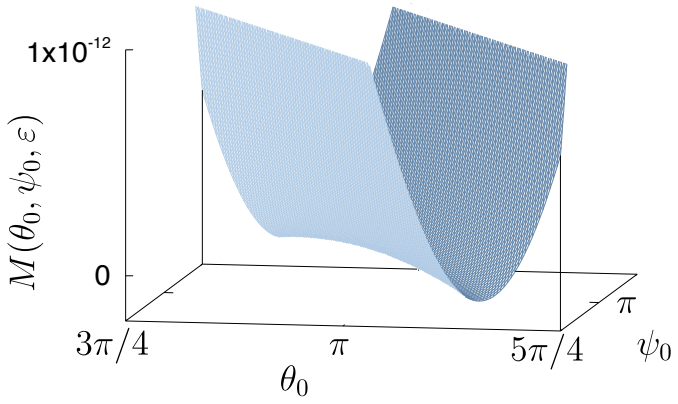

Figure 16: We display the Melnikov function for $\varepsilon \approx \varepsilon_*$, where there is a change of the dominant harmonic of the Melnikov function and, at $(\theta_0, \psi_0) = (\pi, \pi)$, a quadratic tangency of saddle type occurs between the 2D invariant manifolds. Accordingly, the graph of the Melnikov function is locally a hyperbolic paraboloid.

(a) all combinations $m_1\psi_0 + m_2\theta_0$ appear in the Fourier expansion of X_1 along the unperturbed invariant manifold of X_0,

(b) and there are $\rho_\theta, \rho_\psi > 0$ such that the amplitude of the (m_1, m_2)-Fourier coefficient decays, at least, as $\sim \exp(-m_1\rho_\theta - m_2\rho_\psi)$, asymptotically for ε small enough.

The decay of the Fourier coefficients required above includes the possibility of having an entire function in X_1, as is the case of the example considered in this paper. The full spectrum assumption implies that, in particular, trigonometric polynomial perturbations of X_0 do not belong to $\mathcal{U}_X$. However, general periodic perturbations of a system X_0 having an integrable bubble of stability, such that it remains as a non-integrable bubble of stability after the perturbation, are expected to be given by vector fields of $\mathcal{U}_X$. The following result applies to the class of systems $\mathcal{U}_X$ above.

Theorem 5.1. *Consider a system $X = X_0 + \delta X_1 \in \mathcal{U}_X$ and δ small enough and fixed. Assume that the asymptotic behaviour (as $\varepsilon \to 0$) of the splitting of the 2D invariant manifolds of the saddle-foci $p_\pm$ is given by the first order in δ Melnikov approximation M. Moreover, assume that there exists $\varepsilon_0 > 0$ such that M_2 is a dominant approximation for all $\varepsilon < \varepsilon_0$. Then,*

1) There is a decreasing sequence $\{\varepsilon_j\}_j \to 0$ of values of ε for which M_2 has two critical saddle points. In a range of values of ε near ε_j there are two quadratic heteroclinic tangencies of saddle type between the 2D invariant manifolds $W^u(p_+)$ and $W^s(p_-)$.

2) If $\omega = [a_0; \bar{a}] = [a_0; a, a, \cdots]$, $a_0 \in \mathbb{Q}$, then $\varepsilon_{j+1}/\varepsilon_j \to (\omega + a - a_0)^2$ as $j \to 0$.

Proof. Consider an ε-interval $I_\varepsilon = (\varepsilon_n, \varepsilon_m)$, with $\varepsilon_m < \varepsilon_0$, such that there is $\varepsilon_* \in I_\varepsilon$ where a change of the leading harmonic, from the harmonic (m_1, m_2) to the harmonic (n_1, n_2) (as ε decreases), takes place. By assumption, the dominant part of the Melnikov function for $\varepsilon \in (\varepsilon_n, \varepsilon_m)$ is M_2.

Under assumption (A3.b), the Cauchy theorem implies that the negative logarithm of the contribution of a (k_1, k_2)-harmonic related to the k-th best approximant of ω is given by a quantity that behaves as $k_2 + (\varepsilon k_2 c_k)^{-1}$, where $c_k = c_{k_1,k_2}$ is the constant in (14). Then, by Theorem 1 in [19], it follows that

- no two consecutive harmonics related to best approximants can be hidden and,
- if there is a hidden harmonic related to the k-th best approximant of ω, then the next quotient a_{k+1} in its CFE is equal to 1.

It follows from the previous assertions that the linear change $\alpha = m_1\theta_0 + m_2\psi_0$, $\beta = n_1\theta_0 + n_2\psi_0$, is given by a unimodular matrix A either if m_1/m_2 and n_1/n_2 are consecutive best approximants of ω or there is a hidden best approximant in between. To see the previous claim, denote p_k/q_k as the k-th best approximant of ω. If m_1/m_2 and n_1/n_2 are consecutive best approximants, this is a well known property of the CFE apparatus, see for example [28]. Otherwise, if the k-th best approximant is related to a hidden harmonic, that is, if $p_{k+1} = m_1$, $q_{k+1} = m_2$, $p_{k-1} = n_1$ and $q_{k-1} = n_2$, then $\det A = p_{k+1}q_{k-1} - p_{k-1}q_{k+1} = a_{k+1}(p_kq_{k-1} - p_{k-1}q_k) = \pm 1$ because $a_{k+1} = 1$.

Then $\tilde{M}_2 = M_2 \circ A$ can be written as

$$\tilde{M}_2(\alpha, \beta) = \hat{C}_{m_1,m_2}(\varepsilon)e^{i\alpha} + \hat{C}_{n_1,n_2}(\varepsilon)e^{i\beta},$$

where $\hat{C}_{m_1,m_2}(\varepsilon), \hat{C}_{n_1,n_2}(\varepsilon) \in \mathbb{C}$. From (A3.b) and because the change of leading harmonic takes place for $\varepsilon \in (\varepsilon_n, \varepsilon_m)$, it follows that $C_{m_1,m_2} = |\hat{C}_{m_1,m_2}(\varepsilon)|$ is monotonically increasing and $C_{n_1,n_2} = |\hat{C}_{n_1,n_2}(\varepsilon)|$ is monotonically decreasing in the range of ε considered. Let $\theta_1, \theta_2 \in [0, 2\pi)$ such that

$$\tilde{M}_2(\alpha, \beta) = C_{m_1,m_2}T(\alpha, \theta_1) + C_{n_1,n_2}T(\beta, \theta_2),$$

where $T(\alpha, \theta) = \cos^2(\theta)\cos(\alpha) + \sin^2(\theta)\sin(\beta)$. Note that $|T(\alpha, \theta)| \leq 1$, and it has a unique maximum and minimum, where it reaches the values $+1$ and -1, respectively. Then M_2 has two critical points of saddle type. If p_c is a critical point of M_2 of saddle type, the condition $\tilde{M}_2(p_c) = 0$ requires $C_{m_1,m_2} = C_{n_1,n_2}$. Moreover, p_c is non-degenerate since the determinant of the Hessian matrix does not vanish. As ω has bounded CFE, assumption (A3.a) guarantees that there are infinitely many changes of dominant harmonic as $\varepsilon \to 0$ and the reasoning above implies the existence of the sequence $\{\varepsilon_j\}_j \to 0$. As M_2 is dominant for $\varepsilon < \varepsilon_0$ and we assume that the splitting is given by δM, by the implicit function theorem two quadratic tangencies between the 2D invariant manifolds of the saddle-foci are expected for two values of $\varepsilon \approx \varepsilon_j$ for each j. This proves 1).

Under the assumptions (A1)-(A3), a direct application of the Cauchy theorem shows that the contribution C_{m_1,m_2} of the (m_1, m_2)-harmonic to the Melnikov function M is

$C_{m_1,m_2} \sim \exp(-m_1\rho_\theta - |m_2|\rho_\psi)\exp(-s\pi/2\varepsilon)$ if both f and g are non-entire analytic,

$C_{m_1,m_2} \sim \frac{1}{m_1!}\exp(-|m_2|\rho_\psi)\exp(-s\pi/2\varepsilon)$ if f is entire and g is non-entire analytic,

$C_{m_1,m_2} \sim \frac{1}{m_2!}\exp(-|m_1|\rho_\theta)\exp(-s\pi/2\varepsilon)$ if f is non-entire analytic and g is entire,

$C_{m_1,m_2} \sim \frac{1}{m_1!m_2!}\exp(-s\pi/2\varepsilon)$ if both f and g are entire.

Recall that we have considered ω of constant type for assertion 2). Then, as m_1/m_2 is a best approximant, there is a constant $\gamma > 0$ such that $s \sim \gamma/m_2$. The largest contribution to M is given by $m_1, m_2 \sim 1/\sqrt{\varepsilon}$, from where one obtains $C_{m_1,m_2} \sim \exp(-1/\sqrt{\varepsilon})$ if f, g are both non-entire analytic, and $C_{m_1,m_2} \sim \exp(-\sqrt{|\log\varepsilon|/\varepsilon})$ otherwise. In particular, there exists a function $F(\varepsilon)$ such that $\|F(\varepsilon)\log C_{m_1,m_2}\|_\infty$ tends to a constant as $\varepsilon \to 0$ and, moreover, $F(\varepsilon) = O(\sqrt{\varepsilon})$ when both f and g are non-entire analytic functions and $F(\varepsilon) = O(\sqrt{\varepsilon/|\log\varepsilon|})$ otherwise.

The assertion 2) is a consequence of the fact that, given $j \geq 1$, there is $\tilde{\varepsilon}_j \in (\varepsilon_{j+1}, \varepsilon_j)$ where the maximum of $\tilde{F}(s, \varepsilon) = F(\varepsilon)\log C_{m_1,m_2} \approx -sF(\varepsilon)\varepsilon^{-1}$ is achieved. Then, if $\log\Delta_j = \log\varepsilon_j - \log\varepsilon_{j+1}$ and $\log\tilde{\Delta}_j = \log\tilde{\varepsilon}_j - \log\tilde{\varepsilon}_{j+1}$, one has $|\log\Delta_j - \log\tilde{\Delta}_j| \to 0$ as $\varepsilon \to 0$. Hence, it is enough to measure the distance between consecutive maxima of the function $\tilde{F}(s, \varepsilon)$. Let

$s_m = |m_2\omega - m_1| \approx \gamma/m_2$ and $s_n = |n_2\omega - n_1| \approx \gamma/n_2$, where γ is the Diophantine constant. From $\tilde{F}(s_m, \tilde{\varepsilon}_j) = \tilde{F}(s_m, \tilde{\Delta}_j\tilde{\varepsilon}_{j+1}) = \tilde{F}(s_n, \tilde{\varepsilon}_{j+1})$ one obtains

$$\frac{s_m}{s_n} = \frac{\tilde{\Delta}_j F(\tilde{\varepsilon}_{j+1})}{F(\tilde{\Delta}_j\tilde{\varepsilon}_{j+1})},$$

which leads to $\Delta_j = (s_m/s_n)^2$ if $F(\varepsilon) = \mathcal{O}(\sqrt{\varepsilon})$ and to $\Delta_j = (s_m/s_n)^2(1 + \mathcal{O}(|\log\tilde{\varepsilon}_{j+1}|^{-1}))$ if $F(\varepsilon) = O(\sqrt{\varepsilon/|\log\varepsilon|})$. On the other hand, if $\omega = [a_0; a, a, \dots]$ and $m_1/m_2, n_1/n_2$ are the consecutive best approximants of ω of order $k-1$ and k, then

$$\frac{s_m}{s_n} = \frac{|m_2\omega - m_1|}{|n_2\omega - n_1|} \approx \frac{n_2}{m_2} = [a; a..., a] \to \omega + a - a_0 \quad \text{as } k \to +\infty,$$

and we obtain that $\Delta_j = \varepsilon_{j+1}/\varepsilon_j \to (\omega + a - a_0)^2$ asymptotically when $j \to +\infty$. □

In agreement with to the second statement of Theorem 5.1, for $\omega = \sqrt{2} = [1; \bar{2}]$, we see in Fig. 8 right and in Fig.10 that the asymptotic distance $\log(\varepsilon_{j+1}) - \log(\varepsilon_j)$ tends to $2\log(\omega + 1)$ as $\varepsilon \to 0$.

The previous theorem gives a description of the zero-level curve of the Melnikov function in a small neighbourhood of the quadratic tangencies of saddle type. In order to explain the evolution of the level curve for any $\varepsilon < \varepsilon_0$ we study the variation of the angle of the oriented tangent direction at the curve. In particular, we are interested in points where the angle changes by $\approx \pi$ since they are related to oscillations in the level curve. Let $I_\varepsilon = (\varepsilon_n, \varepsilon_m)$, with $\varepsilon_m < \varepsilon_0$, and assume that for $\varepsilon_* \in I_\varepsilon$ there is a change of the leading harmonic. We show below that there are values $\varepsilon_*^{\psi_0}, \varepsilon_*^{\theta_0}$ with $\varepsilon_* < \varepsilon_*^{\psi_0} < \varepsilon_*^{\theta_0} < \varepsilon_m$ such that the angle at $\varepsilon_*^{\theta_0}$ is zero and at $\varepsilon_*^{\psi_0}$ is $\pi/2$, see Fig. 17.

For $\varepsilon \in I_\varepsilon$, $C_{m_1,m_2}(\varepsilon)$ is monotonically increasing while $C_{n_1,n_2}(\varepsilon)$ is decreasing. Therefore, we can consider $\epsilon := \epsilon(\varepsilon) \in [0, 1]$ such that $C_{m_1,m_2} = C\epsilon$ and $C_{n_1,n_2} = C(1-\epsilon)$. Note that when ϵ is either 0 or 1, M_1 is a dominant approximation of M with harmonics (n_1, n_2) and (m_1, m_2) respectively. For $\epsilon = 1/2$, the amplitudes of both Fourier harmonics coincide and there is a quadratic tangency between the invariant manifolds, as shown in the previous theorem.

We consider points $(\theta_*, \psi_*) \in \{M_2 = 0\}$ such that, for all ϵ, $T_1(m_1\theta_* + m_2\psi_*) = 0$ and $T_2(n_1\theta_* + n_2\psi_*) = 0$, and so $T_1'(m_1\theta_* + m_2\psi_*) = \pm 1$ and $T_2'(n_1\theta_* + n_2\psi_*) = \pm 1$. The tangent direction can vary greatly at those points when changing $\epsilon \in [0, 1]$. A tangent vector v at (θ_*, ψ_*) is given by $DM_2(\theta_0, \psi_0, \varepsilon)\, v = 0$. Taking into account the signs of T_1', T_2' and $\hat{C}_{m_1,m_2}, \hat{C}_{n_1,n_2}$, one can check that at those points, the angle of the tangent vector at (θ_*, ψ_*) is either $\xi_1(\epsilon) = \operatorname{atan2}(m_1\epsilon - n_1 + n_1\epsilon, -m_2\epsilon + n_2 - n_2\epsilon)$ or $\xi_2(\epsilon) = \operatorname{atan2}(-m_1\epsilon - n_1 + n_1\epsilon, m_2\epsilon + n_2 - n_2\epsilon)$. Consequently, as ϵ goes from 0 to 1, ξ_1 monotonically increases/decreases from $-\arctan(n_1/n_2)$ to $\pi - \arctan(m_1/m_2)$ and ξ_2 monotonically decreases/increases from $-\arctan(n_1/n_2)$ to $-\arctan(m_1/m_2)$. Then, if $\varsigma = \operatorname{sign}(\hat{C}_{m_1,m_2}\hat{C}_{n_1,n_2})$, the largest variation of the angle takes place at those points (θ_*, ψ_*) with $T_1(m_1\theta_* + m_2\psi_*) = T_2(n_1\theta_* + n_2\psi_*) = 0$ where $\varsigma \neq \operatorname{sign}(T_1'(m_1\theta_* + m_2\psi_*)\, T_2'(n_1\theta_* + n_2\psi_*))$.

6 Behaviour of some local quantities related to the splitting of the 2D invariant manifolds

This last section is devoted to describe the asymptotic behaviour of two local observables, the *splitting Σ-area* and the *splitting angle*. By *local observable* we refer to quantities that are com-

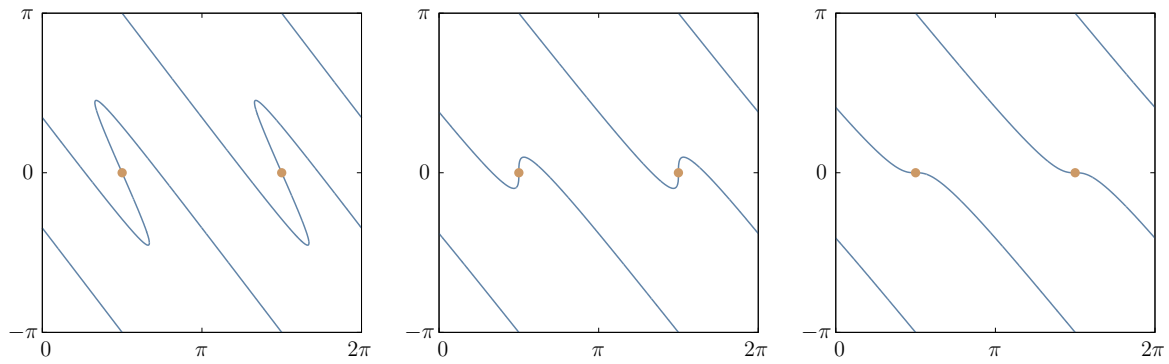

Figure 17: For $\omega = \sqrt{2}$, we display $\{M_2 = 0\}$ for $\log \varepsilon \approx -3.4067, -3.3550$ and -3.3105, which correspond to $\epsilon = 0.55$, $\epsilon_*^{\psi_0} = 0.\bar{6}$ and $\epsilon_*^{\theta_0} = 0.75$. For $\log(\varepsilon_*) \approx -3.42536$, or equivalently for $\epsilon_* = 0.5$, there is a change of leading harmonic from $(m_1, m_2) = (1, 1)$ to $(n_1, n_2) = (3, 2)$, and one has $\varsigma > 0$. The marked points are $(\pi/2, 0)$ and $(3\pi/2, 0)$.

puted along a concrete heteroclinic orbit. The asymptotic behaviour of these local observables can be used as a guide to describe the asymptotic behaviour of the splitting of the 2D invariant manifolds of discrete near-integrable volume-preserving maps (under suitable hypothesis that leads to similar quasi-periodic phenomena). In particular, from a numerical point of view, local observables based on local computations at a heteroclinic point (like the splitting angle or the Lazutkin invariant) can be accurately approximated with moderate computational effort, in contrast to those quantities involving more global computations (like the area of homo/heteroclinic lobes or the splitting/Melnikov function).

As explained in Section 3, the intersection $\mathcal{T}^{u/s}$ of the invariant manifolds $W^u(p_-)$ and $W^s(p_+)$ with $\Sigma = \{z = 0\}$ can be expressed as a graph $\mathcal{G}^{u/s}$ over $\mathcal{T}$, such that $\mathcal{T}^{u/s} = \mathcal{G}^{u/s}(\mathcal{T})$. In particular, given $(\theta_*, \psi_*) \in \mathcal{T}$ such that $S_\delta(\theta_*, \psi_*, \varepsilon) = 0$, the point $p_* = \mathcal{G}^u(\theta_*, \psi_*) = \mathcal{G}^s(\theta_*, \psi_*) \in \Sigma$ corresponds to the intersection with Σ of a heteroclinic orbit between p_- and p_+ of the vector field (1). To measure the splitting of the invariant manifolds W^u and W^s at the heteroclinic point p_* we define the *splitting* Σ*-area* and the *splitting angle* between the invariant manifolds as suitable (local) observables.

The *splitting* Σ*-area at* $p_* \in \Sigma$, that we denoted below as $\mathcal{A}(p_*)$, is the signed area of the parallelepiped that form the normalized tangent vectors to the curves $\mathcal{T}^u \cap \{\psi = \psi_*\}$ and $\mathcal{T}^s \cap \{\psi = \psi_*\}$ at p_*. We recall that the invariant manifolds $W^u(p_-)$ and $W^s(p_+)$ intersect along a continuum of heteroclinic orbits. We refer to [29] for a general description of a similar situation for 3D volume-preserving maps. The *splitting angle* $\alpha(p_*)$ is the angle between the two tangent planes at p_*.

First, we consider the splitting Σ-area. Assume that the invariant manifolds $W^u(p_-)$ and $W^s(p_+)$ intersect transversally along the heteroclinic orbit corresponding to p_*. To compute $\mathcal{A}(p_*)$ it is convenient to introduce coordinates (H, θ_0, ψ_0) in Σ where $(\theta_0, \psi_0) \in \mathcal{T}$ and $H = H_\varepsilon(0, r) - H_\varepsilon(p_0^s)$, where $H_\varepsilon(z, r)$ is defined in (6). Therefore, $\mathcal{T}^s$ corresponds to $\{H = 0\}$ while $\mathcal{T}^u$ is mapped onto $\{H = \mathcal{S}_\delta(\theta_0, \psi_0, \varepsilon),\ (\theta_0, \psi_0) \in \mathcal{T}\}$. The heteroclinic point p_* has coordinates $(0, \theta_*, \psi_*)$. Moreover, the tangent space to W^s at the point p_* is mapped onto the linear subspace generated by the vectors $v_1^\top = (0, 1, 0)$ and $v_2^\top = (0, 0, 1)^\top$ and, since $S_\delta(\theta_0, \psi_0, \varepsilon) = \delta M(\theta_0, \psi_0, \varepsilon) + \mathcal{O}(\delta^2)$, the tangent space to W^s at p_* corresponds to the linear space generated by $u_1^\top = (\delta \partial_{\theta_0} M(\theta_*, \psi_*, \varepsilon) + \mathcal{O}(\delta^2), 1, 0)^\top$ and $u_2^\top = (\delta \partial_{\psi_0} M(\theta_*, \psi_*, \varepsilon) + \mathcal{O}(\delta^2), 0, 1)^\top$. Then,

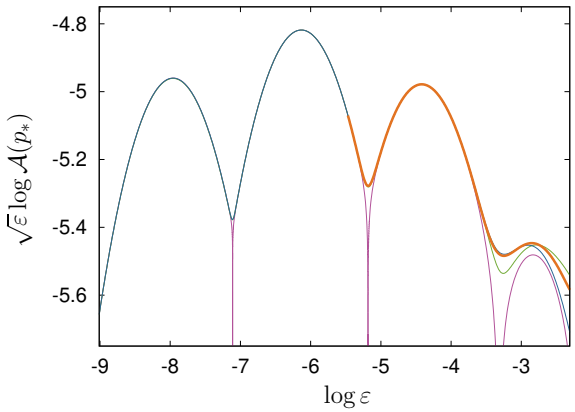

Figure 18: Behaviour of $\sqrt{\varepsilon}\log|\mathcal{A}(p_*)|$ for different values of p_* corresponding to $(\theta_*,\psi_*) = (\pi/2,\pi)$ in blue, $(\theta_*,\psi_*) = (\pi/2,0)$ in purple and $(\theta_*,\psi_*) = (\theta_*(\varepsilon),\pi/2)$ in green (this is obtained by continuation, see text for details). We also display in orange the direct numerical computation of $\mathcal{A}(p_*)$ for $p_* = (\pi/2,\pi)$.

assuming $\partial_{\theta_0}M(\theta_*,\psi_*,\varepsilon) \neq 0$, the vectors v_1 and u_1 generate $\{\psi = \psi_*\}$ and

$$\mathcal{A}(p_*) = \frac{1}{\|v_1\|\|u_1\|}\left|\det\begin{pmatrix}0 & \delta\partial_{\theta_0}M + \mathcal{O}(\delta^2)\\ 1 & 1\end{pmatrix}\right| = \delta\,\frac{|\partial_{\theta_0}M|}{\sqrt{(\delta\partial_{\theta_0}M)^2+1}} + \mathcal{O}(\delta^2),$$

where $\partial_{\theta_0}M = \partial_{\theta_0}M(\theta_*,\psi_*,\varepsilon)$.

We display in Fig.18 the splitting Σ-area $\mathcal{A}(p_*)$ for different values of ε in the heteroclinic orbit $(\theta_*,\psi_*) = (\pi/2,\pi)$ (in blue), in $(\theta_*,\psi_*) = (\pi/2,0)$ (in purple), and in the heteroclinic orbit obtained by continuation with respect to ε of the heteroclinic orbit with $\psi_* = \pi/2$ fixed and $\theta_* = \theta_*(\varepsilon)$ such that $\theta_*(0.1) \approx \pi$ (in green). In the same figure, we superpose (in orange) the values obtained from a direct numerical computation of $\mathcal{A}(p_*)$ for $(\theta_*,\psi_*) = (\pi/2,\pi)$, hence obtained from the propagation of tangent vectors up to Σ to obtain a basis of the tangent spaces to $W^u(p_-)$ and to $W^s(p_+)$ at p_*. We note that the splitting Σ-area have similar quasi-periodic exponentially small behaviour with respect to ε as the splitting function studied in Section 4.

Note that the splitting Σ-area for the heteroclinic with $(\theta_*,\psi_*) = (\pi/2,0)$ is zero for some values of ε, because the slope of the tangent direction to the continuum of heteroclinics at this point is zero for this value of ε, as explained at the end of Section 5. The tangent slope in this heteroclinic point is given by the function $\xi_1(\epsilon)$, see Fig. 17 right.

We now consider the splitting angle $\alpha(p_*)$. This is a natural quantity to measure the splitting between the invariant manifolds for a discrete map. Note that $F = \phi^T$ is the Poincaré map to the section $\Sigma_{\psi_*} = \{\psi = \psi_*\}$. We illustrate in Fig. 19 the splitting angle between the invariant manifolds at $p_* = (\pi/2,\pi)$.

We observe in the figure that the splitting angle coincides with the Σ-area for some values of ε. In this heteroclinic, the slope of the tangent to the continuum of heteroclinic orbits in $\Sigma = \{z = 0\}$ is given by the function $\xi_2(\epsilon)$ and, when changing from one dominant harmonic to the other one, it crosses $-\omega$. The Poincaré map from Σ to Σ_ψ maps a vector with slope $-\omega$ to a vertical vector in coordinates (θ_0, z). Then, at these values of ε, the tangent vector to the continuum of heteroclinic orbits is normal to $\{z = 0\}$ in Σ_ψ. This happens at each ε-interval where there is a change of leading harmonic of the Melnikov function, see Theorem 5.1.

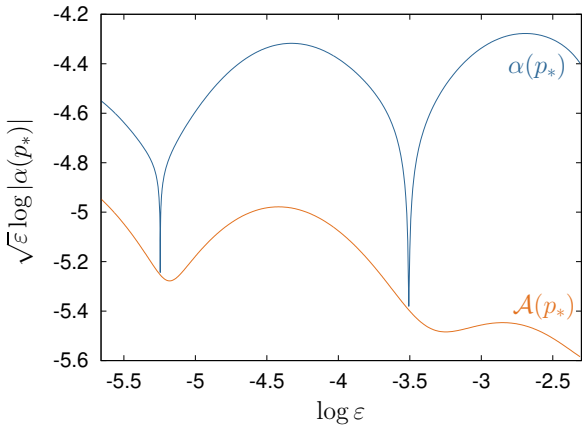

Figure 19: Behaviour of the splitting angle $\alpha(p_*)$ and the splitting Σ-area $\mathcal{A}(p_*)$ for $p_* = (\pi/2, \pi)$.

7 Conclusions

We have studied a δ-periodic forcing of a 3D conservative vector field that corresponds to a second-order normal form of the ε-unfolding of a Hopf-zero bifurcation at $\varepsilon = 0$. For δ small and fixed, we have described the asymptotic behaviour, as $\varepsilon \to 0$, of the splitting of the 2D invariant manifolds of the saddle-foci points that arise at the bifurcation. Assuming δ small we have given numerical evidence that the splitting of those manifolds behaves exponentially small in ε. The scenario here considered is of the lowest possible dimension to have such an interaction of internal and external frequencies. The concrete example studied is general enough to exhibit the richness of the quasi-periodic phenomena of the splitting while simple enough to obtain explicit analytic expressions of the leading terms of the Melnikov functions and explicit bounds of the ignored terms. The role of the interaction of the internal frequency (related to the rotational symmetry of the integrable system) with the external frequency (coming from the periodic forcing) in the splitting behaviour has been analysed and illustrated.

We are confident that the (universal) properties of the asymptotic behaviour of the splitting of the 2D invariant manifolds reported here can be useful to study similar settings. In particular, it would be interesting to consider a physical fluid model to investigate the change of a bubble shape due to a periodic forcing, [27], and where the behaviour here described could be observed. On the other hand, it could be interesting to consider non-perturbative regimes. In this sense, high order Taylor-Fourier expansions [9, 25, 34] combined with adapted computer assisted techniques to validate the Melnikov approximation [7] can be useful. Also, a similar behaviour has been observed for the splitting of the 2D invariant manifolds of discrete near-integrable volume-preserving maps with similar geometry and under suitable hypotheses and will be reported elsewhere. Note that the theoretical description of the asymptotic behaviour of the splitting relies on the proper identification of the frequencies interacting which, for general maps, are expected to change when changing the parameters of a generic family of maps.

Finally, it is well-known that the splitting of separatrices is a source of complex (chaotic) dynamics around the invariant manifolds. The emerging richness of dynamics in 2D area-preserving maps has been widely studied, but for 3D (and higher dimensional) maps, a detailed description of the dynamics within the chaotic zone is still missing. The splitting phenomena discussed here are genuinely higher-dimensional and may contribute to investigate the main features within chaotic zones in this setting, such as the location of resonant islands, the size of the chaotic zone, the bifurcations that take place, etc. The asymptotic behaviour of the Melnikov function

(which gives the first order of the splitting function) that we provide here is a key ingredient to derive a suitable separatrix-like return map [10, 37, 41] adapted to this setting.

A Upper bound of the amplitude of a harmonic of the Melnikov function

The Melnikov function defined in (11) is given by

$$M(\theta_0, \psi_0, \varepsilon) = \sum_{m_2 \in \mathbb{Z}} \sum_{m_1 \geq 0} \hat{C}_{m_1,m_2}\, T(m_1\theta_0 + m_2\psi_0),$$

where $T(\alpha) = \cos(\alpha)$ if m_1 is odd and $T(\alpha) = \sin(\alpha)$ otherwise, and

$$C_{m_1,m_2} = |\hat{C}_{m_1,m_2}| = \frac{2^5\pi\varrho_d^{|m_2|}}{\sqrt{d^2-1}c^{m_1}} \sum_{i\geq 0} \frac{(m_1+2i)!}{c^{2i}(m_1+2i+4)!(m_1+i)!i!}\, \frac{1}{h(s)}\, P_{m_1+2i+4}(s,\varepsilon).$$

with $s = |m_2\omega - m_1|$, $h(s) = \cosh\left(\frac{s\pi}{2\varepsilon}\right)$ if m_1 is odd and $h(s) = \sinh\left(\frac{s\pi}{2\varepsilon}\right)$ otherwise.

Recall that P_k are defined recursively as $P_0(s,\varepsilon) = 1, P_1(s,\varepsilon) = s$ and, for all $k \geq 2$, $P_k(s,\varepsilon) = (s^2 + \varepsilon^2(k-2)^2)P_{k-2}(s,\varepsilon)$. Note that $|P_k(s,\varepsilon)| = P_k(s,\varepsilon)$ verify the same recurrence.

Lemma A.1.

- *For $s \leq \varepsilon$ one has $P_k(s,\varepsilon) \leq (s^2+\varepsilon^2k^2)^{\lfloor k/2\rfloor}\exp(-k)\exp(\frac{s\pi}{2\varepsilon})$.*
- *For $s > \varepsilon$ one has $P_k(s,\varepsilon) \leq (s^2+\varepsilon^2k^2)^{\lfloor k/2\rfloor}$.*

Proof. For $k \geq 2$, a straightforward computation gives

$$\log P_k(s,\varepsilon) = \log(s^2+\varepsilon^2(k-2)^2) + \log P_{k-2}(s,\varepsilon) = \sum_{j=k-2(-2)a} \log(s^2+\varepsilon^2j^2)$$
$$\leq \frac{1}{2}\int_a^k \log(s^2+\varepsilon^2j^2)dj = \log s(k-a) + \frac{s}{4\varepsilon}\int_{z_{min}}^{z_{max}} \frac{\log(1+z)}{\sqrt{z}}dz,$$

where $a = 1$ if k is odd and $a = 0$ otherwise, $z = \varepsilon^2j^2/s^2$, $z_{min} = (a\varepsilon/s)^2$ and $z_{max} = (k\varepsilon/s)^2$. Thus, for any k, the direct evaluation of the last integral gives

$$\log P_k(s,\varepsilon) \leq \lfloor k/2\rfloor \log(s^2+\varepsilon^2k^2) - k + \frac{s}{\varepsilon}\arctan(k\varepsilon/s) + C,$$

where $C = 1 - \arctan(\varepsilon/s)\, s/\varepsilon - 1/2\log(s^2+\varepsilon^2) + \log(s) < 0$ if k is odd and $C = 0$ otherwise. □

Remark A.1. The error in the upper bound of $\log P_k$ for $s > \varepsilon$ is the sum of the error $E_1 \approx \log(1 + \varepsilon^2k^2/s^2)/2$ due to the approximation of the sum by the integral, and the error $E_2 \approx k^3\varepsilon^2/(3s^2)$ because the approximation $(s/\varepsilon)\arctan(k\varepsilon/s) \approx k$.

A.1 Contribution of the terms with $s \leq \varepsilon$.

We bound the contribution to $|M(\theta_0, \psi_0, \varepsilon)|$ of the terms with $s \leq \varepsilon$. Note that, as $\omega > 0$, these terms must have $m_1 > 0$ (as $m_1 = 0$ leads to the contradiction $\omega < \varepsilon$) and $m_2 > 0$ (otherwise, $1 \leq m_1 \leq m_1 - m_2\omega = s \leq \varepsilon$ is a contradiction). Moreover, we assume that $\omega > 0$ satisfies a Diophantine condition of the form $s = |m_2\omega - m_1| \geq \gamma_2 |m_2|^{-\tau}$ with $\tau \geq 1$ and $\gamma_2 > 0$.

From the previous lemma, we obtain the following upper bound for the Melnikov function

$$|M(\theta_0, \psi_0, \varepsilon)| \leq \frac{2^5\pi}{\sqrt{d^2-1}e^4} \sum_{m_2 \geq 1} \varrho_d^{m_2} \sum_{m_1 \geq 1} \sum_{i \geq 0} \frac{(m_1+2i)!(s^2+\varepsilon^2(m_1+2i+4)^2)^{(m_1+2i+4)/2}\, \mathcal{S}(\frac{s\pi}{2\varepsilon})}{c^{m_1+2i}e^{m_1+2i}(m_1+2i+4)!(m_1+i)!i!},$$

where $\mathcal{S}(x) = e^x/\sinh(x)$ for m_1 odd and $\mathcal{S}(x) = e^x/\cosh(x)$ otherwise.

Lemma A.2. *Under the previous assumptions, if $0 < \gamma_1 \leq \gamma_2\omega^\tau$, one has*

(i) $s \geq \gamma_1 m_1^{-\tau}$,

(ii) $\mathcal{S}(\frac{s\pi}{2\varepsilon}) \leq \frac{8}{\gamma_1\pi}\varepsilon m_1^\tau$.

Proof. To prove (i) it is enough to look for γ_1 such that $\gamma_2 m_2^{-\tau} \geq \gamma_1 m_1^{-\tau}$ or, equivalently, $\gamma_1(m_2/m_1)^\tau \leq \gamma_2$. Since $s < \varepsilon$ and $m_1 \geq 1$ one has

$$\frac{m_2}{m_1} \leq \left|\frac{m_2}{m_1} - \frac{1}{\omega}\right| + \frac{1}{\omega} = \frac{1}{\omega}\left(\frac{s}{m_1}+1\right) < \frac{1}{\omega}\left(\frac{\varepsilon}{m_1}+1\right) < \frac{1}{\omega}(\varepsilon+1) < \frac{1}{\omega},$$

then $\gamma_1(m_2/m_1)^\tau \leq \gamma_1/\omega^\tau$, and we see that $\gamma_1 \leq \gamma_2\omega^\tau$ guarantees $s \geq \gamma_1 m_1^{-\tau}$.

To prove (ii) note that, as the function $x\mathcal{S}(x)$ is increasing on $x > 0$, then $x\mathcal{S}(x) \leq (\pi/2)\mathcal{S}(\pi/2) < 4$ for all $0 < x < \pi/2$. Taking $x = s\pi/(2\varepsilon)$, since $s \geq \gamma_1 m_1^{-\tau}$, it follows the bound. □

Let $\nu_1 = \gamma_1/\varepsilon$ and $\nu_2 = \gamma_2/\varepsilon$, it follows from (i) that $m_1 > \lfloor \nu_1 \rfloor^{1/\tau} = \nu_1^*$ and $m_2 > \lfloor \nu_2 \rfloor^{1/\tau} = \nu_2^*$.

Lemma A.3. *Under the previous assumptions, for any $\varepsilon < \varepsilon_1^0 = \min(\frac{c}{24e}, \frac{\gamma_1}{(\tau+1)^\tau+1})$, one has*

$$|M_{s\leq\varepsilon}(\theta_0, \psi_0, \varepsilon)| \leq \frac{2^5 c(c\sqrt{2\pi}+\gamma_1)}{3\pi e^4(1-\varrho_d)\sqrt{d^2-1}\varrho_d}\, \gamma_1^{\frac{4-\tau}{2\tau}}\, \varepsilon^{\frac{5\tau+4}{2\tau}} \exp\left(-\frac{\gamma_1^{1/\tau}\left(|\log(24\varepsilon/c)| + |\log\varrho_d|/\omega\right)}{\varepsilon^{1/\tau}}\right).$$

Proof. For any $\varepsilon < \varepsilon_1^0$ and any $i \geq 0$, one has $s^2 + \varepsilon^2(m_1+2i+4)^2 \leq \varepsilon^2(m_1+2i+4)^2(1+m_1^{-2}) \leq \varepsilon^2(m_1+2i+4)^2(1+(\nu_1^*)^{-2}) \leq 2\varepsilon^2(m_1+2i+4)^2$, then

$$|M_{s\leq\varepsilon}(\theta_0, \psi_0, \varepsilon)| \leq \frac{2^{11}3\varepsilon^5}{\gamma_1 e^4\sqrt{d^2-1}} \sum_{m_2 > \nu_2^*} \varrho_d^{m_2} \sum_{m_1 > \nu_1^*} \sum_{i \geq 0} A(m_1, i),$$

where

$$A(m_1, i) = \left(\frac{\varepsilon}{ce}\right)^{m_1+2i} \frac{m_1^\tau(\sqrt{2}(m_1+2i+4))^{m_1+2i}}{(m_1+i)!i!}.$$

Let $k = m_1 + i$. We write $A(m_1, i) = A(m_1, k-m_1) = \left(\frac{\varepsilon}{ce}\right)^{2k} \frac{1}{k!} 2^k \tilde{A}(m_1, k)$, where

$$\tilde{A}(m_1, k) = \left(\frac{\varepsilon}{ce}\right)^{-m_1} \frac{m_1^\tau(2k-m_1+4)^{2k-m_1}}{(k-m_1)!}.$$

Then,

$$|M_{s\le\varepsilon}(\theta_0,\psi_0,\varepsilon)| \le \frac{2^{11}3\varepsilon^5\varrho_d^{\nu_2^*}}{\gamma_1 e^4(1-\varrho_d)\sqrt{d^2-1}} S_K$$

where

$$S_K = \sum_{k>\nu_1^*}\left(\frac{\sqrt{2}\,\varepsilon}{c\,e}\right)^{2k}\frac{1}{k!}S_{\tilde{A}}, \qquad \text{and} \qquad S_{\tilde{A}} = \sum_{m_1=\nu_1^*}^{k}\tilde{A}(m_1,k). \tag{24}$$

Our goal is to bound S_K by an exponentially small quantity of the form $\sim \exp(-C/\varepsilon^\nu)$ with $C>0$ and $\nu \ge \nu_0 > 1/2$. First, we have

$$\tilde{A}(k,k) = \left(\frac{ce}{\varepsilon}\right)^k k^\tau (k+4)^k.$$

On the other hand, $S_{\tilde{A}} - \tilde{A}(k,k) = \sum_{m_1=\nu_1^*}^{k-1}\tilde{A}(m_1,k)$. Using Stirling's approximation[3] one gets

$$\sum_{m_1=\nu_1^*}^{k-1}\tilde{A}(m_1,k) \le \frac{e^k}{\sqrt{2\pi}}\sum_{m_1=\nu_1^*}^{k-1}\left(\frac{\varepsilon}{c}\right)^{-m_1}\frac{m_1^\tau(2k-m_1+4)^{2k-m_1}}{\sqrt{k-m_1}(k-m_1)^{k-m_1}} \le \frac{e^k}{\sqrt{2\pi}}\left(\frac{c}{\varepsilon}\right)^{k-1}(k-1)^\tau\sum_{m_1=1}^{k-1}f(m_1),$$

where $f(x) = (2k-x+4)^{2k-x}/(k-x)^{k-x}$. This function is bounded by $f(x) \le f(1) = (2k+3)^{2k-1}/(k-1)^{k-1} \le 4^k(k+4)^k$, since it is decreasing in $[1,k-1]$ and $k\ge 2$, which holds for $\varepsilon \le \gamma_1/((\tau+1)^\tau+1)$. Then

$$\sum_{m_1=\nu_1^*}^{k-1}\tilde{A}(m_1,k) \le \frac{e^k}{\sqrt{2\pi}}\left(\frac{c}{\varepsilon}\right)^{k-1}(k-1)^{\tau+1}6^k(k+2)^k \le \frac{\varepsilon}{c\sqrt{2\pi}}\left(\frac{4ce}{\varepsilon}\right)^k(k-1)^{\tau+1}(k+4)^k.$$

We conclude that

$$S_K \le \sum_{k>\nu_1^*}\left(\frac{2\varepsilon}{ce}\right)^k\frac{(k+4)^k}{k!}\left[k^\tau + \frac{\varepsilon}{c\sqrt{2\pi}}k^{\tau+1}4^k\right].$$

Using Stirling's approximation and that $(k+4)/k \le 1+4/\nu_1^* \le 3$ one gets

$$S_K \le \frac{\sqrt{\varepsilon}}{\sqrt{2\pi\gamma_1}}\left(\sum_{k>\nu_1^*}k^\tau R_1^k + \frac{\varepsilon}{c\sqrt{2\pi}}\sum_{k>\nu_1^*}k^{\tau+1}R_2^k\right),$$

where $4R_1 = R_2 = \frac{24\varepsilon}{c} \le e^{-1} < 1$. Next, we use Lemma A.4 below to bound S_K by

$$S_K \le \frac{2\sqrt{\varepsilon}}{\sqrt{2\pi\gamma_1}}\left(1+\frac{\gamma_1}{c\sqrt{2\pi}}\right)\left(\frac{24\varepsilon}{c}\right)^{\nu_1^*-1}{\nu_1^*}^{\mathcal{T}+1},$$

where $\mathcal{T}\in\mathbb{Z}$ is the smallest integer number such that $\tau\le\mathcal{T}$. Therefore, the contribution to the Melnikov function of the terms with $s\le\varepsilon$ is bounded by

$$\begin{aligned}|M_{s\le\varepsilon}(\theta_0,\psi_0,\varepsilon)| &\le \frac{2^8\varepsilon^3\sqrt{\varepsilon}(c\sqrt{2\pi}+\gamma_1)}{\pi\sqrt{\gamma_1}\,e^4(1-\varrho_d)\sqrt{d^2-1}}\varrho_d^{\left\lfloor\frac{\gamma_2}{\varepsilon}\right\rfloor^{1/\tau}}\left(\frac{24\varepsilon}{c}\right)^{\left\lfloor\frac{\gamma_1}{\varepsilon}\right\rfloor^{1/\tau}}\left(\frac{\gamma_1}{\varepsilon}\right)^{2/\tau}\\ &\le A\varepsilon^B\exp\left(-\left(\frac{\gamma_1}{\varepsilon}\right)^{1/\tau}(|\log(24\varepsilon/c)| + |\log\varrho_d|/\omega)\right)\end{aligned}$$

where $A = \frac{2^5c(c\sqrt{2\pi}+\gamma_1)}{3\pi e^4(1-\varrho_d)\sqrt{d^2-1}\varrho_d}\gamma_1^{\frac{4-\tau}{2\tau}}$ and $B = \frac{5\tau+4}{2\tau}$. □

[3] Stirling's approximation: $\frac{1}{n!} \le \frac{\exp(-1/(12n+1))}{\sqrt{2\pi n}}\left(\frac{e}{n}\right)^n \le \frac{1}{\sqrt{2\pi n}}\left(\frac{e}{n}\right)^n$, for any $n\ge 1$.

Lemma A.4. *Let $\mathcal{T} \in \mathbb{Z}$ be the smallest integer number such that $\tau \leq \mathcal{T}$. For any $0 < R \leq e^{-1}$, one has*

$$\sum_{k>\nu_1^*} k^{\tau+1} R^k \leq 2R^{\nu_1^*-1} {\nu_1^*}^{\mathcal{T}+2}.$$

Proof. Given $\varepsilon \leq \gamma_1/((\tau+1)^\tau+1)$ and $R \leq e^{-1}$, $k > \nu_1^*$ implies that $k \geq (\tau+1)/|\log(R)|$. The function $k^{\tau+1}R^k$ is decreasing for $k \geq (\tau+1)/|\log(R)|$ and we can bound

$$\sum_{k>\nu_1^*} k^{\tau+1} R^k \leq \int_{\nu_1^*-1}^{\infty} x^{\tau+1} R^x dx \leq \int_{\nu_1^*-1}^{\infty} x^{\mathcal{T}+1} R^x dx.$$

Let $I_{\mathcal{T}+1} = \int_{\nu_1^*-1}^{\infty} x^{\mathcal{T}+1} R^x dx = (\nu_1^*-1)^{\mathcal{T}+1} \frac{R^{\nu_1^*-1}}{|\log(R)|} + \frac{\mathcal{T}+1}{|\log(R)|} I_{\mathcal{T}}$, with $I_0 = R^{\nu_1^*-1}/|\log(R)|$. Then,

$$\begin{aligned} I_{\mathcal{T}+\infty} &= \frac{R^{\nu_1^*-1}}{|\log(R)|} \left[(\nu_1^*-1)^{\mathcal{T}+1} + (\mathcal{T}+1) \sum_{i=1}^{\mathcal{T}} (\nu_1^*-1)^i |\log(R)|^{i-\mathcal{T}-1} \right] \\ &\leq \frac{R^{\nu_1^*-1}}{|\log(R)|} (\nu_1^*-1)^{\mathcal{T}} \left[\nu_1^* - 1 + \mathcal{T}(\mathcal{T}+1) |\log(R)|^{-1} \right]. \end{aligned}$$

□

Remark A.2. Note that for $\tau = 1$, the sum $\sum_{k>\nu_1^*} k^2 R^k$ can be directly computed and so the bound of $|M_{s\leq\varepsilon}(\theta_0, \psi_0, \varepsilon)|$ can be slightly improved without using the bound of Lemma A.4.

A.2 Contribution of the terms with $s \geq \varepsilon^\alpha$, $\alpha \leq 1/2 - \eta$, $\eta > 0$

We bound the contribution to $|M(\theta_0, \psi_0, \varepsilon)|$ of the terms with $s \geq \varepsilon^\alpha$, $\alpha \leq 1/2 - \eta$, $\eta > 0$. For any $s > \varepsilon$ one has $P_k(s, \varepsilon) \leq (s^2 + \varepsilon^2 k^2)^{\lfloor k/2 \rfloor}$ from Lemma A.1 and for s/ε sufficiently large, we can approximate $1/h(s)$ by $2\exp\left(-\frac{s\pi}{2\varepsilon}\right)$ to provide the upper bound

$$|M_{s>\varepsilon^\alpha}(\theta_0, \psi_0, \varepsilon)| \leq \frac{2^6\pi}{\sqrt{d^2-1}} \sum_{m_2 \in \mathbb{Z}} \varrho_d^{|m_2|} S(m_1, i)$$

where

$$S(m_1, i) = \sum_{m_1 \geq 0} \sum_{i \geq 0} \exp\left(-\frac{s\pi}{2\varepsilon}\right) A_{m_1,i}, \quad \text{and } A_{m_1,i} = \frac{(m_1+2i)!(s^2+\varepsilon^2(m_1+2i+4)^2)^{\lfloor (m_1+2i+4)/2 \rfloor}}{c^{m_1+2i}(m_1+2i+4)!(m_1+i)!i!}.$$

Lemma A.5. *Under the previous assumptions, for any $\varepsilon < \varepsilon_2^0 = \min(\frac{1}{2^4}, \frac{c}{20\sqrt{2e}})$, one has*

$$|M_{s\geq\varepsilon^\alpha}(\theta_0, \psi_0, \varepsilon)| \leq K \exp\left(-\frac{\pi}{2\varepsilon^{1/2+\eta}}\right),$$

for some positive constant $K \in \mathbb{R}$ and $\eta > 0$.

Proof. Let $i_{s,m_1} = \lfloor \frac{1}{2}\left(\frac{s}{\varepsilon} - m_1 - 4\right) \rfloor$. The term $s^2 + \varepsilon^2(m_1+2i+4)^2$ is bounded by $2s^2$ if $i \geq 0$ and $i \leq i_{s,m_1}$, and by $2\varepsilon^2(m_1+2i+4)^2$ otherwise. Accordingly, we split $S(m_1, i) = S(m_1, i \leq i_{s,m_1}) + S(m_1, i > i_{s,m_1})$.

First we deal with the term $S(m_1, i > i_{s,m_1})$. Note that $i_{s,m_1} \leq 0$ if $s \leq (m_1+4)\varepsilon$. Let $i_{\min}^{s,m_1} = \max(i_{s,m_1}+1, 0)$ and introduce $k = m_1 + i$. The terms in $S(m_1, i > i_{s,m_1})$ are those with $k \geq 1$ because, otherwise, $s^2 \geq \varepsilon^2(m_1+2i+4)^2$ for $\varepsilon < \varepsilon_2^0$. Then one has

$$\begin{aligned} S(m_1, i > i_{s,m_1}) &\leq \frac{2^7}{3}\varepsilon^4 \exp\left(-\frac{\pi}{2\varepsilon^{1-\alpha}}\right) \sum_{m_1\geq 0} \sum_{i\geq i_{\min}^{s,m_1}} \left(\frac{\sqrt{2}\varepsilon}{c}\right)^{m_1+2i} \frac{(m_1+2i+4)^{m_1+2i}}{(m_1+i)!i!} \\ &\leq \frac{2^7}{3}\varepsilon^4 \exp\left(-\frac{\pi}{2\varepsilon^{1-\alpha}}\right) \sum_{k\geq 1} \left(\frac{\sqrt{2}\varepsilon}{c}\right)^{2k} \frac{1}{k!} \sum_{m_1=0}^{k} \left(\frac{\sqrt{2}\varepsilon}{c}\right)^{-m_1} \frac{(2k-m_1+4)^{2k-m_1}}{(k-m_1)!} \end{aligned}$$

Note the similarity with S_K in (24): if one replaces m_1^τ by 1 they only differ in the ranges of m_1 and k. Indeed, performing the analogous estimates in this simpler case one obtains that, for $\varepsilon < \varepsilon_2^0$, there is a constant $K_1 \geq 0$ such that,

$$S(m_1, i > i_{\min}^{s,m_1}) \leq K_1 \exp\left(-\frac{\pi}{2\varepsilon^{1-\alpha}}\right).$$

Next we consider the case $S(m_1, i \leq i_{s,m_1})$. We write $S(m_1, i \leq i_{s,m_1}) = S_\alpha(m_1, i \leq i_{s,m_1}) + \sum_{j\geq 1} S_j(m_1, i \leq i_{s,m_1})$, where $S_\alpha = S_\alpha(m_1, i \leq i_{s,m_1})$ (resp. $S_j = S_j(m_1, i \leq i_{s,m_1})$) denotes the terms with $\varepsilon^\alpha \leq s < 1$ (resp. with $j \leq s < j+1$). Let $\Upsilon_j = \sqrt{2}c^{-1}(j+1)$. Using that $(m_1+i)! \geq m_1!i!$ it follows that

$$S_j \leq \frac{(j+1)^4}{6} \exp\left(-\frac{j\pi}{2\varepsilon}\right) \sum_{m_1\geq 0} \frac{(\Upsilon_j)^{m_1}}{m_1!} \sum_{i\geq 0} \left(\frac{(\Upsilon_j)^i}{i!}\right)^2 = \frac{(j+1)^4}{6} \exp\left(-\frac{j\pi}{2\varepsilon} + \Upsilon_j\right) I_0(2\Upsilon_j), \tag{25}$$

where I_0 is the modified Bessel function of the first kind. Since $I_0(x) \leq \exp(x)$ for all $x \geq 0$, then

$$S_j \leq \frac{(j+1)^4}{6} \exp\left(-\frac{j\pi}{2\varepsilon} + 3\Upsilon_j\right) \leq C_1 \exp\left(-C_2\frac{j}{\varepsilon}\right).$$

where $C_1 = \exp(3\sqrt{2}c^{-1})/6$ and $C_2 = \pi/2 - (3\sqrt{2}c^{-1}+4)\varepsilon$. Then, taking ε small enough

$$\sum_{j\geq 1} S_j \leq 2C_1 \exp(-C_2/\varepsilon).$$

Finally, the analogous to (25) for S_α implies

$$S_\alpha \leq \frac{1}{6} \exp\left(-\frac{\pi}{2\varepsilon^{1-\alpha}}\right) \sum_{m_1\geq 0} \frac{(\sqrt{2}c^{-1})^{m_1}}{m_1!} \sum_{i\geq 0} \left(\frac{(\sqrt{2}c^{-1})^i}{i!}\right)^2 \leq \frac{C_1}{6} \exp\left(-\frac{\pi}{2\varepsilon^{1-\alpha}}\right).$$

We conclude that, for $\alpha \leq 1/2 - \eta$ with $\eta > 0$, there is a constant $K_2 \geq 0$ such that

$$S(m_1, i \leq i_{s,m_1}) \leq K_2 \exp\left(-\frac{\pi}{2\varepsilon^{1/2+\eta}}\right).$$

Therefore, the contribution to the Melnikov function of the terms with $s \geq \varepsilon^\alpha$ is bounded by

$$|M_{s\geq\varepsilon^\alpha}(\theta_0, \psi_0, \varepsilon)| \leq \frac{2^6\pi(\varrho_d+1)}{\sqrt{d^2-1}(1-\varrho_d)}(K_1+K_2) \exp\left(-\frac{\pi}{2\varepsilon^{1/2+\eta}}\right).$$

□

Acknowledgements

A.V. and A.M. are supported by the Spanish grant PID2021-125535NB-I00 funded by MICIU/AEI/10.13039/501100011033 and by ERDF/EU. A.M. grant PID2021-125535NB-I00 is also funded by "ESF+". A.V. and A.M. also acknowledge the Catalan grant 2021-SGR-01072. A.V. also acknowledges the Severo Ochoa and María de Maeztu Program for Centers and Units of Excellence in R&D (CEX2020-001084-M).

References

[1] I. Baldomá, O. Castejón, and T. M. Seara. Breakdown of a 2D heteroclinic connection in the Hopf-zero singularity (I). *J. Nonlinear Sci.*, 28(5):1551–1627, 2018.

[2] I. Baldomá, S. Ibáñez, and T. M. Seara. Hopf-zero singularities truly unfold chaos. *Commun. Nonlinear Sci. Numer. Simul.*, 84:105162, 19, 2020.

[3] C. Batut, K. Belabas, D. Bernardi, H. Cohen, and M. Olivier. *Users' guide to PARI/GP.* http://pari.math.u-bordeaux.fr/.

[4] X. Cabré, E. Fontich, and R. de la Llave. The parameterization method for invariant manifolds. I. Manifolds associated to non-resonant subspaces. *Indiana Univ. Math. J.*, 52(2):283–328, 2003.

[5] X. Cabré, E. Fontich, and R. de la Llave. The parameterization method for invariant manifolds. II. Regularity with respect to parameters. *Indiana Univ. Math. J.*, 52(2):329–360, 2003.

[6] X. Cabré, E. Fontich, and R. de la Llave. The parameterization method for invariant manifolds. III. Overview and applications. *J. Differential Equations*, 218(2):444–515, 2005.

[7] M. J. Capiński and P. Zgliczyński. Beyond the Melnikov method: a computer assisted approach. *J. Differential Equations*, 262(1):365–417, 2017.

[8] J.W.S. Cassels. *An introduction to Diophantine approximation*, volume No. 45 of *Cambridge Tracts in Mathematics and Mathematical Physics*. Cambridge University Press, New York, 1957.

[9] R. Castelli, J.P. Lessard, and J. D. Mireles James. Parameterization of invariant manifolds for periodic orbits I: Efficient numerics via the Floquet normal form. *SIAM J. Appl. Dyn. Syst.*, 14(1):132–167, 2015.

[10] B.V. Chirikov. A universal instability of many-dimensional oscillator system. *Phys. Rep.*, 52:264 – 379, 1979.

[11] A. Delshams, V. Gelfreich, A. Jorba, and T. M-Seara. Exponentially small splitting of separatrices under fast quasiperiodic forcing. *Communications in Mathematical Physics*, 189:35–71, 10 1997.

[12] A. Delshams, M. Gonchenko, and P. Gutiérrez. Continuation of the exponentially small transversality for the splitting of separatrices to a whiskered torus with silver ratio. *Regul. Chaotic Dyn.*, 19(6):663–680, 2014.

[13] A. Delshams, M. Gonchenko, and P. Gutiérrez. Exponentially small asymptotic estimates for the splitting of separatrices to whiskered tori with quadratic and cubic frequencies. *Electron. Res. Announc. Math. Sci.*, 21:41–61, 2014.

[14] A. Delshams, M. Gonchenko, and P. Gutiérrez. Exponentially small lower bounds for the splitting of separatrices to whiskered tori with frequencies of constant type. *Internat. J. Bifur. Chaos Appl. Sci. Engrg.*, 24(8):1440011, 12, 2014.

[15] A. Delshams and P. Gutiérrez. Exponentially small splitting for whiskered tori in Hamiltonian systems: continuation of transverse homoclinic orbits. *Discrete Contin. Dyn. Syst.*, 11(4):757–783, 2004.

[16] A. Delshams and P. Gutiérrez. Exponentially Small Splitting of Separatrices for Whiskered Tori in Hamiltonian Systems. *Journal of Mathematical Sciences*, 128(2):2726 –2745, 2005.

[17] F. Dumortier, S. Ibáñez, H. Kokubu, and C. Simó. About the unfolding of a Hopf-zero singularity. *Discrete Contin. Dyn. Syst.*, 33(10):4435–4471, 2013.

[18] M. Feingold, L.P. Kadanoff, and O. Piro. Passive scalars, three-dimensional volume-preserving maps, and chaos. *J. Statist. Phys.*, 50(3-4):529–565, 1988.

[19] E. Fontich, C. Simó, and A. Vieiro. On the "hidden" harmonics associated to best approximants due to quasi-periodicity in splitting phenomena. *Regul. Chaotic Dyn.*, 23(6):638–653, 2018.

[20] E. Fontich, C. Simó, and A. Vieiro. Splitting of the separatrices after a Hamiltonian–Hopf bifurcation under periodic forcing. *Nonlinearity*, **32**(4):1440–1493, 2019.

[21] N.K. Gavrilov. Bifurcations of an equilibrium state with one zero root and a pair of purely imaginary roots and additional degeneration. In *Methods of the qualitative theory of differential equations (Russian)*, pages 43–51. Gor'kov. Gos. Univ., Gorki, 1987.

[22] J. Guckenheimer. On a codimension two bifurcation. In *Dynamical systems and turbulence, Warwick 1980 (Coventry, 1979/1980)*, volume 898 of *Lecture Notes in Math.*, pages 99–142. Springer, Berlin-New York, 1981.

[23] À. Haro, M. Canadell, J-Ll. Figueras, A. Luque, and J.M. Mondelo. *The parameterization method for invariant manifolds*, volume 195 of *Applied Mathematical Sciences*. Springer, [Cham], 2016. From rigorous results to effective computations.

[24] P. Holmes. Some remarks on chaotic particle paths in time-periodic, three-dimensional swirling flows. In *Fluids and plasmas: geometry and dynamics (Boulder, Colo., 1983)*, volume 28 of *Contemp. Math.*, pages 393–404. Amer. Math. Soc., Providence, RI, 1984.

[25] G. Huguet, R. de la Llave, and Y. Sire. Computation of whiskered invariant tori and their associated manifolds: new fast algorithms. *Discrete Contin. Dyn. Syst.*, 32(4):1309–1353, 2012.

[26] A. Jorba and M. Zou. A software package for the numerical integration of ODEs by means of high-order Taylor methods. *Experiment. Math.*, 14(1):99–117, 2005.

[27] I. S. Kang and L. G. Leal. Bubble dynamics in time-periodic straining flows. *J. Fluid Mech.*, 218:41–69, 1990.

[28] A.Y. Khinchin. *Continued Fractions*. The University of Chicago Press, Chicago, Ill.-London, 1964.

[29] H.E. Lomelí and R. Ramírez-Ros. Separatrix splitting in 3D volume-preserving maps. *SIAM J. Appl. Dyn. Syst.*, 7(4):1527–1557, 2008.

[30] I. Mezic. *On the geometrical and statistical properties of dynamical systems: Theory and applications*. ProQuest LLC, Ann Arbor, MI, 1994. Thesis (Ph.D.)–California Institute of Technology.

[31] K.C. Miles, B. Nagarajan, and D.A. Zumbrunnen. Three-dimensional chaotic mixing of fluids in a cylindrical cavity. *Trans. ASME: J. Fluids Engng*, 117:582–588, 1995.

[32] J. D. Mireles James and H. Lomelí. Computation of heteroclinic arcs with application to the volume preserving Hénon family. *SIAM J. Appl. Dyn. Syst.*, 9(3):919–953, 2010.

[33] B.A. Mosovsky and J.D. Meiss. Transport in transitory, three-dimensional, Liouville flows. *SIAM J. Appl. Dyn. Syst.*, 11(4):1785–1816, 2012.

[34] M. Murray and J. D. Mireles James. Computer assisted proof of homoclinic chaos in the spatial equilateral restricted four-body problem. *J. Differential Equations*, 378:559–609, 2024.

[35] A. Neishtadt, C. Simó, and A. Vasiliev. Geometric and statistical properties induced by separatrix crossings in volume-preserving systems. *Nonlinearity*, 16(2):521–557, 2003.

[36] A.I. Neishtadt and A.A. Vasiliev. Change of the adiabatic invariant at a separatrix in a volume-preserving 3D system. *Nonlinearity*, 12(2):303–320, 1999.

[37] G.N. Piftankin and D.V. Treschev. Separatrix maps in Hamiltonian systems. *Russian Math. Surveys IOP*, 2(62):219–322, 2007.

[38] D.A. Salamon. The Kolmogorov-Arnold-Moser theorem. *Math. Phys. Electron. J.*, 10:Paper 3, 37, 2004.

[39] C. Simó. Averaging under fast quasiperiodic forcing. *Hamiltonian Mechanics: Integrability and Chaotic Behavior*, Springer US:13–34, 1994.

[40] C. Simó and C. Valls. A formal approximation of the splitting of separatrices in the classical arnold's example of diffusion with two equal parameters. *Nonlinearity*, 14(6):1707, oct 2001.

[41] C. Simó and A. Vieiro. Dynamics in chaotic zones of area preserving maps: close to separatrix and global instability zones. *Physica D*, 240(8):732–753, 2011.

[42] M.F.M. Speetjens, H.J.H. Clercx, and G.J.F. van Heijst. A numerical and experimental study on advection in three-dimensional Stokes flows. *J. Fluid Mech.*, 514:77–105, 2004.

[43] R. Sturman, S.W. Meier, J.M. Ottino, and S. Wiggins. Linked twist map formalism in two and three dimensions applied to mixing in tumbled granular flows. *J. Fluid Mech.*, 602:129–174, 2008.

[44] F. Takens. Singularities of vector fields. *Inst. Hautes Études Sci. Publ. Math.*, 43:47–100, 1974.

[45] D.L. Vainchtein, J. Widloski, and R.O. Grigoriev. Mixing properties of steady flow in thermocapillary driven droplets. *Physics of Fluids*, 19(6):067102, 06 2007.